ImmunoHorizons, 2025, **9(2)**, vlae007
https://doi.org/10.1093/immhor/vlae007
Research Article

Combination adjuvant improves influenza virus immunity by downregulation of immune homeostasis genes in lymphocytes

Emmanuel Dollinger [1,], Jenny Hernandez-Davies [2,**], Jiin Felgner [2], Aarti Jain [2], Michael Hwang [2], Erwin Strahsburger [2], Rie Nakajima [2], Algimantas Jasinskas [2], Qing Nie [1], Egest James Pone [2], Shivashankar Othy [2], and David Huw Davies [2,*]**

[1]Department of Mathematics, University of California Irvine, Irvine, CA, United States
[2]Vaccine Research & Development Center, Department of Physiology & Biophysics, University of California Irvine, Irvine, CA 92697, United States

*Corresponding author: Vaccine Research & Development Center, Department of Physiology & Biophysics, University of California Irvine, 812 Medical Plaza Drive, Med Surge II, Irvine, CA 92693, United States. Email: ddavies@uci.edu.

**These authors contributed equally to the work.

Abstract

Adjuvants play a central role in enhancing the immunogenicity of otherwise poorly immunogenic vaccine antigens. Combining adjuvants has the potential to enhance vaccine immunogenicity compared with single adjuvants, although the cellular and molecular mechanisms of combination adjuvants are not well understood. Using the influenza virus hemagglutinin H5 antigen, we define the immunological landscape of combining CpG and MPLA (TLR-9 and TLR-4 agonists, respectively) with a squalene nanoemulsion (AddaVax) using immunologic and transcriptomic profiling. Mice immunized and boosted with recombinant H5 in AddaVax, CpG+MPLA, or AddaVax plus CpG+MPLA (IVAX-1) produced comparable levels of neutralizing antibodies and were equally well protected against the H5N1 challenge. However, after challenge with H5N1 virus, H5/IVAX-1–immunized mice had 100- to 300-fold lower virus lung titers than mice receiving H5 in AddaVax or CpG+MPLA separately. Consistent with enhanced viral clearance, unsupervised expression analysis of draining lymph node cells revealed the combination adjuvant IVAX-1 significantly downregulated immune homeostasis genes, and induced higher numbers of antibody-producing plasmablasts than either AddaVax or CpG+MPLA. IVAX-1 was also more effective after single-dose administration than either AddaVax or CpG+MPLA. These data reveal a novel molecular framework for understanding the mechanisms of combination adjuvants, such as IVAX-1, and highlight their potential for the development of more effective vaccines against respiratory viruses.

Keywords: combination adjuvant, influenza, lymphocytes, single-cell transcriptomics, synergy

Introduction

Subunit vaccines based on recombinant proteins are inherently safer than live attenuated vaccines and offer many advantages for at-scale manufacture and lot-to-lot consistency. However, recombinant proteins are poorly immunogenic and require adjuvants to engender a robust and durable immune response.[1,2] Aluminum salts (alum) have been widely used as adjuvants since the 1930s, when they were first shown to enhance the immune response to tetanus and diphtheria toxoids (reviewed recently).[3] Billions of doses of vaccines adjuvanted with alum have been since administered safely to humans, and it remains the most widely used adjuvant in current vaccines. The adjuvant effect of alum is thought to reside in the particulate nature of aluminum salts, and its capacity to activate the inflammasome and a T helper 2 (Th2)–polarized humoral response.[4] However, alum does not stimulate a robust Th1 response, which is needed for effective immunity against intracellular pathogens, and until relatively recently, alum was also the only adjuvant approved for human use.

In the early 2000s, the first generation of vaccines that exploited ligands of innate microbial sensing receptors as adjuvants, such as toll-like receptor (TLR) agonists, were first approved.[5] TLR agonists operate through a common signaling pathway mediated through MyD88 and TRIF (except for TLR3, which is MyD88 independent and TRIF mediated), resulting in the initiation of a complex signaling cascade culminating in the activation of nuclear factor kappa B (NF-κB) and initiation of innate and adaptive immune responses.[6,7] Next generation adjuvants used in approved vaccines include Adjuvant System 1 (AS01) from GlaxoSmithKline, which comprises 3-O-desacyl-4′-monophosphoryl lipid A (MPLA), a nonreactogenic derivative of bacterial lipopolysaccharide, and a plant-derived saponin, QS-21, that acts as a surfactant. These are combined in dioleoyl phosphatidylcholine and cholesterol-based liposomes.[8] MPLA and QS-21 synergize to induce a local inflammatory reaction.[9] AS01 is used in the commercial vaccines Shingrix and Mosquirix (both GlaxoSmithKline) against shingles (herpes zoster) and malaria, respectively. AS04, also developed by GlaxoSmithKline, comprises alum and MPLA, and is used in the vaccine Cervarix, for prevention of human papillomavirus infections and cervical cancers. The only other TLR agonist currently used in approved vaccines is unmethylated oligodeoxynucleotides containing cytosine-guanine dinucleotide motifs (CpG ODN). TLR9 was first cloned and identified as a receptor for

Received: October 23, 2024. **Accepted:** October 23, 2024

CpG 20 years ago,[10] and was subsequently shown to drive a Th1 immune profile.[11–13] CpG-1018 (Dynavax) is used in the current hepatitis B vaccine Heplisav-b. Other TLR agonists, including poly I:C (TLR3 agonist) and imiquimod (TLR7), are currently under intense investigation as adjuvants.

An additional adjuvant family comprises viscoelastic carriers, and in particular emulsions. The first emulsions were water-in-oil (WO), such as Incomplete Freund's Adjuvant, which is a WO emulsion of nonmetabolizable mineral oil. Complete Freund's Adjuvant is mineral oil containing a suspension of killed *Mycobacterium bovis*. While Freund's adjuvants are strongly immunogenic and act as an antigen depot, they are difficult to formulate consistently; require large gauge needles which increase injury at the injection site; and are too reactogenic for human use.[14] Replacing mineral oil with metabolizable vegetable oil (eg, Montanide series of adjuvants) reduces toxicity but nevertheless remains difficult to formulate. Oil-in-water (OW) emulsions are easier to formulate, but the antigen depot effect is likely reduced. The OW emulsion, MF59, is used as an adjuvant in FluAd (Seqirus), a quadrivalent split virion seasonal influenza vaccine designed for persons 65 years of age or older. AS03 (GlaxoSmithKline) is a squalene OW emulsion containing DL-α-tocopherol and polysorbate 80 that has been used in several of GlaxoSmithKline's products, including the inactivated split virion influenza vaccines, Pandemrix, a monovalent H1N1 2009 pandemic influenza vaccine (subsequently withdrawn owing to risk of narcolepsy), and Arepanrix and Q-Pan, both of which are monovalent H5N1 pandemic influenza vaccines. Both MF59 and AS03 squalene OW emulsions are also maintained in the US National Pre-Pandemic Influenza Vaccine Stockpile for use with reserves of influenza pandemic vaccines to be mixed on demand to enhance vaccine immunogenicity and durability, to increase the breadth of antigen recognition, and for possible dose-sparing. The immunostimulatory properties of emulsions are distinct from the pathogen-associated molecular patterns described previously, each of which triggers a specific signal transduction pathway, and are instead thought to be mediated by multimerizing antigen on the micelle surface to enhance receptor crosslinking, acting as an antigen depot to allow for sustained antigen release, or triggering additional responses, such as by causing cell lysis and activation of damage-associated molecular pattern immune pathways.[15]

Our previous studies in the influenza hemagglutinin (HA) H5 model showed that the adjuvanticity of CpG and MPLA are enhanced by combining with squalene nanoemulsion (AddaVax) with an associated shift in the Th1/Th2 response,[16,17] although efficacy was not tested in these studies. Here, we show that mice receiving H5 antigen in AddaVax, CpG+MPLA, or AddaVax plus CpG+MPLA (aka IVAX-1) induce comparable titers of neutralizing antibodies (nAbs), and were protected equally well against H5N1 challenge. However, H5N1 virus lung titers were lower in mice that received the combination adjuvant compared with mice administered emulsion or TLR agonists separately. A transcriptomic analysis of draining lymph nodes 4 d after a boost revealed the combination adjuvant enhanced the downregulation of tumor suppressor and immune homeostasis genes compared with emulsion or TLR agonists alone, which was associated with enhanced immunity, particularly plasmablast numbers. These data indicate that depending on the biological screen, combinations of adjuvants may allow for fine-tuning of immune responses, and may assist in the long-term goal of generating effective and durable protection against multiple pathogen variants.

Materials and methods

Immunizations and challenge studies

Antigen used for immunizations was purified HA subtype H5 from A/Vietnam/1194/2004 expressed in human HEK293 cells (Sino Biological; catalog # 11062-V08H1). Adjuvants used in this study comprised CpG-1018 (Integrated DNA Technologies), MPLA (Avanti Polar Lipids), and the squalene OW emulsion, AddaVax (Invivogen). CpG was dissolved in sterile water at 1 mM as stock, and endotoxin activity of <1 EU/mL was confirmed with LAL Endotoxin Assay Kits (GenScript). MPLA was obtained at >99% purity and incorporated into liposomes of the inert colipid, DOPG (Avanti Polar Lipids), at a 1:5 molar ratio, and is manufactured in organic solvents and has minimal endotoxin activity.

All animal work was approved by the University of Califronia, Irvine Institutional Animal Care and Use Committee Protocols and AUP-21-067 and AUP-21-133. The laboratory animal resources at UCI are Internationally accredited by the Association for Assessment and Accreditation of Laboratory Animal Care (AAALAC #000238). All virus handling was performed in US Department of Agriculture–inspected and approved BSL2+/ABSL2+ facilities. Female C57BL/6 mice (7–10 wk of age) were purchased from Charles River Laboratories, and housed in standard cages with enrichment. Mice for single-cell messenger RNA (mRNA) sequencing analysis and efficacy studies were immunized according to the table shown in Fig. 1A. Five groups of 10 mice were primed and boosted on d28 with different formulations as follows: group 1, phosphate-buffered saline (PBS); group 2, H5/PBS; group 3, H5/AddaVax; group 4, H5/CpG+MPLA; group 5, H5/CpG+MPLA+AddaVax. Each mouse received 5.0 μg H5 antigen administered in a volume of 50 μL via subcutaneous (base of tail) route. Plasma samples were collected on days 14 and 42 for serological analysis by protein microarray and microneutralization assay. Four days after the boost, 3 mice from each group were withdrawn and single cell suspensions of draining (inguinal) lymph nodes prepared for mRNA sequencing using the Chromium (10X Genomics) and Illumina HiSeq systems. The remaining 7 mice from each group were challenged on day 96 with reassortant influenza virus H5N1 (A/Vietnam/1194/2004 × A/Puerto Rico/8/1934) (NIBSC; catalog # NIBRG-14) as described previously.[16] Transiently anesthetized mice were administered 50 μL of virus at 10^4 $TCID_{50}$/mL via the intranasal route and monitored daily for behavior and body weight until the endpoint (day 6 postchallenge), at which time lungs were harvested for viral lung titers by quantitative polymerase chain reaction (qPCR).

Virus lung titers by qPCR

To quantify virus titers, lungs were collected into preweighed cryotubes, snap frozen on dry ice, and stored at −80 °C until required for RNA extraction. Total RNA was extracted by homogenizing weighed lung tissue in 1 ml of TRIzol (Thermo Fisher Scientific) using a GentleMacs Tissue Homogenizer (Miltenyi Biotec) using the preset RNA-01 program, followed

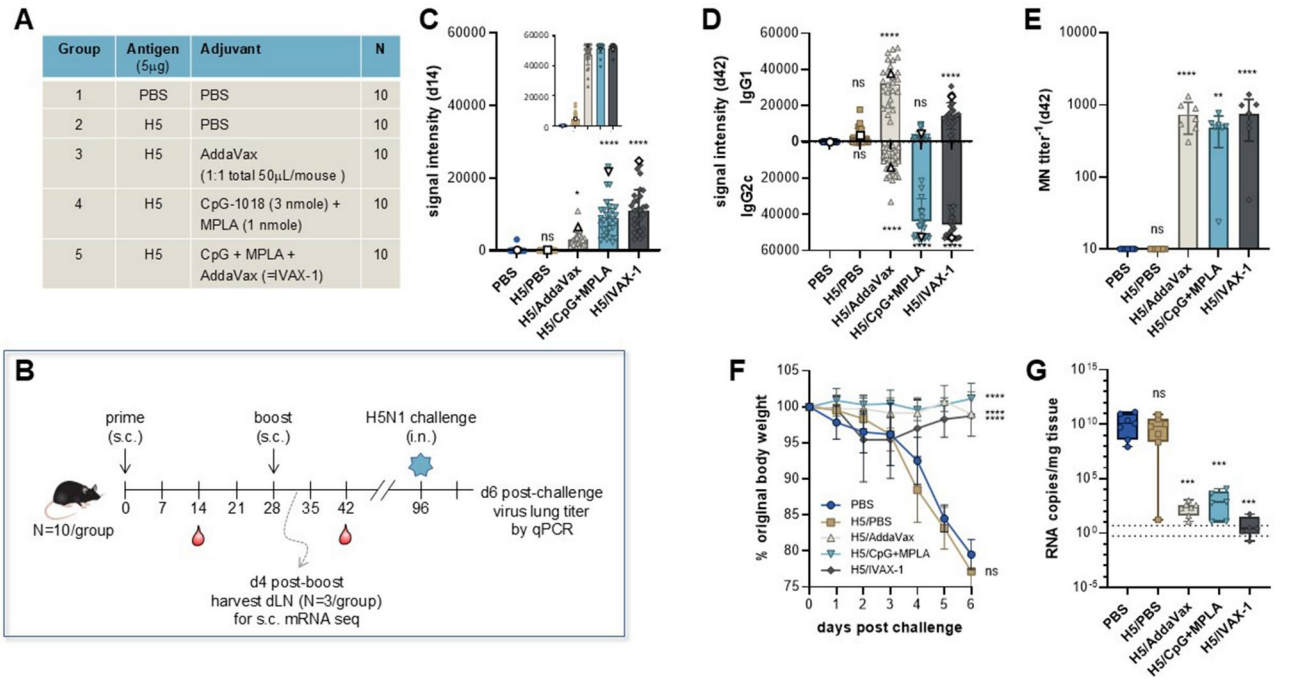

Figure 1. Adjuvant screen in mice. (A) Groups of 10 C57BL/6 female mice were administered H5 (VN04) formulated in IVAX-1 or AddaVax or CpG+MPLA separately, as shown. (B) Timeline; mice received vaccine on d0 and d28 via the subcutaneous route; blood was collected on d14 and d42 for serological analysis. Three mice were withdrawn from each group 4 d postboost for subcutaneous mRNA sequencing analysis of draining lymph nodes (Figs. 3–7) and the remaining 7 mice were challenged on d96 with 50 μL 10^4 $TCID_{50}$ /ml of H5N1 virus matched to the H5 in the vaccine. (C) Magnitude of IgG responses on d14 (preboost) to different H5 drift variants as determined by protein microarray in which each spot is a different H5 drift variant; inset, magnitude of response on d42 (2 weeks postboost); open symbols are the immunizing antigen. (D) IgG1/IgG2c (Th2/Th1) profiles on d42 determined by protein microarray, in which each spot is a different H5 drift variant; open symbols are the immunizing antigen. (E) Microneutralization titers on d42. (F) Normalized body weights (mean ± SD) postchallenge; animals were sacrificed 6 d postchallenge and lungs harvested for virus titers. (G) Lung titers by qPCR. Limit of detection is 10 copies RNA per PCR reaction, which ranges from 0.55 to 5 copies/mg/lung (hashed lines). Significance was calculated using 1-way analysis of variance between the PBS group and each of the other groups using Dunnett's multiple comparisons test. $^{**}P \leq 0.01$; $^{***}P \leq 0.001$; $^{****}P < 0.0001$. i.n., intranasal; ns, nonsignificant, s.c., subcutaneous, s.c. mRNA seq, single-cell messenger RNA sequencing.

by phase separation in Phasemaker tubes and total RNA extraction according to the manufacturer's guidelines (Thermo Fisher Scientific). Total RNA was then resuspended in 100 μL of ultrapure RNAse/DNase-free distilled water and stored at −80 °C. Real-time qPCR (RT-qPCR) amplification was performed according to the World Health Organization guidelines for molecular detection of influenza viruses (https://cdn.who.int/media/docs/default-source/influenza/molecular-detention-of-influenza-viruses/protocols_influenza_virus_detection_feb_2021.pdf). The HA H5 gene was amplified using forward primer NIID-swH1 TMPrimer-F1 (5′-AGAAAAGA ATGTAACAGTAACACACTCTGT-3′), reverse primer NIID-swH1 TMPrimer-R1 (5′-TGTTTCCACAATGTAGG ACCATG-3′0), and TaqMan probe NIID-swH1 probe2 (5′-56-FAM-TGGGTAAAT-ZEN-GTAACATTGCTGGCTG-3′IBkFQ-3′). As a positive amplification control, the housekeeping gene GAPDH from *Mus musculus* was used using primers GADPH-Fw (5′-CAATGTGTCCGTCGTGGATCT-3′), GADPH-Rv (5′-GTCCTCAGTGTAGCCCAAGAT-3′), and the TaqMan probe GADPH probe 5′-SUN-CGTGCCG CC-ZEN-TGGAGAAACCTGCC-3′IABkFQ-3′.[18,19] RT-qPCR was performed using AgPath-ID One-Step RT-PCR Reagents (Thermo Fisher Scientific) following the manufacturer's instructions. Briefly, 20 μL of master mix containing each primer at 0.5 μM, each probe at 0.2 μM, 1× of Q-RT-PCR Master Mix and 1× of QuanTec RT-PCR enzyme mix, plus the inhibitory of RNases (RNaseout; Thermo Fisher Scientific) at 0.4 mM was added to 5 μL of the total extracted RNA and amplified at 50 °C for 10 min, 95 °C for 10 min, and 45 cycles of 95 °C for 10 seconds, 56 °C for 30 seconds (collection data), and 72 °C for 15 seconds. For quantification, an H5 standard curve was produced using $\log_{10}$ serial dilutions of a synthetic linear DNA that contains 1 copy of the H5 gene (8.3×10^7 to 8.3 copies/reaction). A standard curve was generated in parallel with each amplification to estimate the number of H5 copies amplified in each sample. The total copies of H5 gene present in the total RNA extraction were normalized against the weight of lungs (expressed as genomic RNA copies/mg lung).

Immunoassays

Protein microarrays

Magnitude and breadth of antibody response and IgG subtyping were performed using protein microarrays, as described previously.[16,20] Briefly, custom protein microarrays of purified HA and other influenza antigens (purchased from Sino Biological) were printed on nitrocellulose-coated glass slides (Grace Biolabs) using an OmniGrid 100 microarray printer (Genomic Solutions). The content of the array was as reported previously.[21] For probing, plasma samples were diluted 1:100 in blocking buffer (GVS) supplemented with a polyhistidine peptide (Biomatik USA) to final concentration 0.10 μg/mL to block any antibodies to polyhistidine tags. After rehydration, arrays were incubated in diluted plasma overnight at 4 °C, then washed in Tris-buffered saline containing 0.05% Tween 20. Bound IgG was visualized using biotinylated anti-mouse IgG (Jackson ImmunoResearch; Cat. No. 115-068-071), followed after washing by incubation in

streptavidin-conjugated Qdot-800 (Life Technologies; Cat. No. Q10173MP) diluted 1:250 in blocking buffer. For IgG subtyping, anti-mouse IgG1-Alexa Fluor 647 or IgG2c-Alexa Fluor 555 (Southern Biotech; Cat. Nos. 1073-31 and 1077-32) were used as secondary antibodies. After washing and drying, scanned images were acquired using the ArrayCAM imaging system (Grace Bio-Labs). Signal intensities for each antigen on the array were first background-corrected by subtracting sample-specific PBS containing 0.05% Tween 20 buffer signals from purified protein spot signals. Data were plotted and statistical analyses performed using Prism software (GraphPad Software, Version 10.4.1).

Microneutralization assays

Microneutralization (MN) assays were performed as described previously.[16] Briefly, early passage MDCK cells (CCL-34; ATCC) were cultured in Eagle's Minimum Essential Medium (EMEM) with penicillin/streptomycin and 10% heat-inactivated fetal calf serum (FCS) to 80% to 85% confluency. Plasma samples were treated overnight with receptor-destroying enzyme (Denka Seiken) to digest any soluble sialic acid, and then heat-inactivated to denature the receptor-destroying enzyme. Plasma samples were then 2-fold serially diluted from 1/10 to 1/640 in serum-free EMEM containing TPCK-treated trypsin (Worthington Biochemical), and 100 $TCID_{50}$ in 50 μL of H5N1/PR8 virus (NIBRG-14; NIBSC) was added in 50 μL to the equal volume of serially diluted plasma. After 1 h incubation, plasma/virus mixtures were overlaid onto FCS-free MDCK monolayers for 1 h, and then replaced with medium containing 2% heat-inactivated FCS. After 48 h incubation to allow cytopathic effect to develop, cells were fixed in 4% paraformaldehyde, permeabilized in 0.1% PBS/Triton X-100, and blocked in 3% bovine serum albumin. Influenza nucleoprotein was then detected using a cocktail of anti-nucleoprotein monoclonal antibodies (Millipore; Cat. Nos. MAB 8257 and MAB 8258) followed by horseradish peroxidase–conjugated anti-mouse IgG. Plates were developed in TMB peroxidase substrate (SureBlue; KPL), stopped using 0.18 M H_2SO_4 and reaction product quantified in an enzyme-linked immunosorbent assay plate reader. Graphical presentations and statistical analyses were performed in Prism.

Single-cell mRNA sequencing library preparation and data analysis

Single-cell suspensions from draining lymph nodes were filtered through a 45-μm mesh, counted, and loaded at ~ 2,000 cells per microliter, for a total of ~ 20,000 cells per sequencing run following the 10X Geomics manufacturer's recommendations. Cells were obtained from 3 animals per group and sequenced separately. All analyses were performed using scanpy (v1.8.2). For initial quality control, we removed cells with less than 200 sequenced genes and genes sequenced in <3 cells. We then removed cells with more than 10% mitochondrial gene expression. We then removed all mitochondrial and ribosomal genes from the dataset. Data were LogNormalized: the count of each transcript in a cell was divided by the total number of transcripts in that cell, then multiplied by the scale factor (1×10^5). The result was then taken to the natural log plus 1. The following pipeline applies to the results from all figures unless otherwise stated. Genes that were sequenced in <3 cells were removed, then cells were quality controlled again (retaining only cells with more than 400 genes expressed). Features for Fig. 2 were selected using scanpy's highly_variable_genes function with defaults. Features for Figs. 3, 4, and 5 were selected using the BigSur python package (https://github.com/landerlabcode/BigSur). Briefly, BigSur calculates a statistic that accounts for inherent source variation in scRNAseq (called the "modified and corrected Fano factor," or mcFano). Genes were first filtered by mcFano P value ≤ 0.01, then ran the function with min_mcfano_cutoff = false. This causes the feature selection function to calculate silhouette score of clusters calculated from features with different cutoffs of the mcFano (using the default quantile cutoffs from 0.7 to 0.996 with step size of 0.001) and selected the cutoff that resulted in the highest silhouette score. After feature selection, the principal components (PCs) was calculated using scanpy's built in method and retained the top 50 PCs by highest variance explained. Batch correction was performed using the scanpy implementation of harmony, with key = "adjuvant condition." Clusters were then calculated using leiden and visualized using Uniform Manifold Approximation and Projection (UMAP), both using defaults.

Normalization of cell counts

The number of cells in each cell type/state ("cell group") per mouse were summed, then divided by total number of cells per mouse (using pandas value_counts function, with normalize = true).

Differential expression

In order to leverage the number of replicates per condition, the mice were pseudobulked and then differentially expressed genes (DEGs) calculated. We combined the ideas from published methods[22,23] by first pseudobulking, then running Mann-Whitney U (MWU) on the pseudobulked data. Specifically, the counts of each cell group per mouse per gene were summed together, then divided by the total number of counts in that cell group/mouse pair, to create a normalized pseudobulk. We then filtered the genes by how highly expressed they were in the negative control (H5/PBS) to only retain genes that had higher than 1×10^{-4} normalized counts. We then ran MWU on each gene, with groups in most cases H5/PBS vs H5/adjuvant and corrected for multiple testing using Benjamini-Hochberg.

Pseudotime

Pseudotime analyses were performed using the Monocle 3 (v2.18.0) pipeline with defaults, with one exception. We exported the PCs calculated by harmony during the batch correction step and applied the monocle pipeline to those PCs, as opposed to calculating PCs using Monocle. All other steps were held the same: preprocessing using preprocess_cds, cluster cells using cluster_cells, learn the graph using learn_graph (with use_partition = false), and differential expression using Moran's I using graph_test.

Synergy calculations

The synergy score of a gene was defined as the ratio of mean expression in IVAX-1 condition to the sum of the means of gene expression in AddaVax and CpG+MPLA conditions. We assumed that the means of each gene in each condition are equal; therefore, a gene will be synergistic if the ratio of IVAX-1 to the sum of AddaVax and CpG+MPLA is different from 1/2. A positively synergistic gene has higher mean

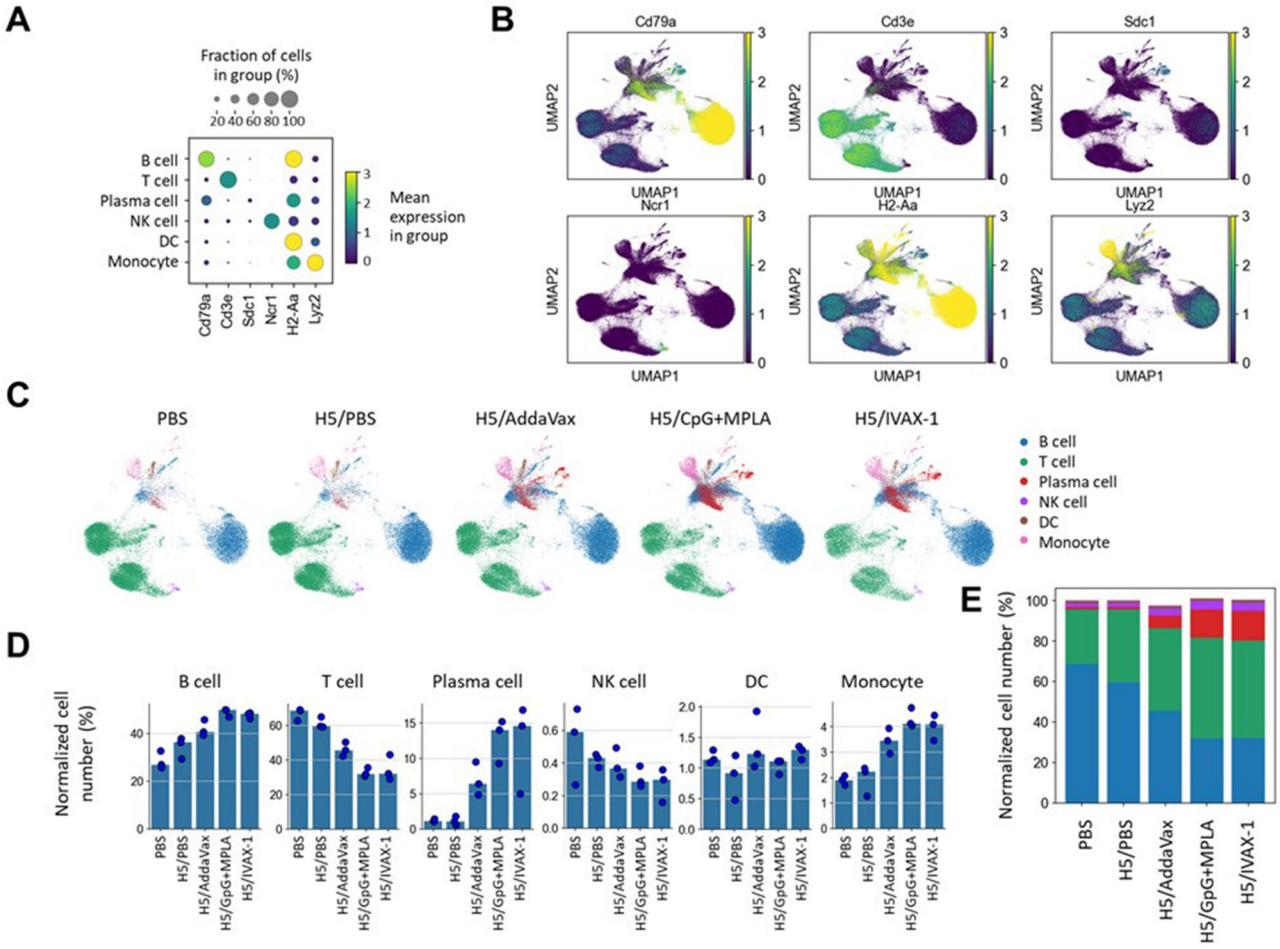

Figure 2. Major immune cell types identified by transcriptomic profiling. (A) Bubble plot showing markers used to identify main immune cell subsets, with expression level and proportion of each marker in each cell subset represented by shade and size of the bubble, respectively. (B) UMAP plots showing major cell subsets and vaccine groups pooled. (C) Location of cell subsets in UMAPs broken out by vaccine group. (D) Bar charts of normalized cell numbers (% of total number of lymph node cells) by vaccine group; each spot represents an individual mouse. (E) Stacked plots of normalized cell counts as shown in panel (C), median of 3 mice.

expression in IVAX-1 than the addition of the means of AddaVax and CpG+MPLA. A negatively synergistic gene has lower mean expression in IVAX-1 than the addition of the means of AddaVax and CpG+MPLA. The log2 of this score was taken for convenience, such that a positively synergistic gene has a score greater than -1, and a negatively synergistic gene has a score <-1. Each mouse replicate was psuedobulked prior to synergy score calculation.

$$synergy_g = log_2\left(\frac{mean(IVAX_g)}{mean(AddaVax_g) + mean(CpG+MPLA_g)}\right)$$

Where g is a given gene. To calculate *P* values for each synergy score, we fit the psuedobulked data to a general linear model with covariate condition:

$$expression_g \sim 0 + condition$$

We then calculated the *P* values for whether the sum of the means of the gene expressions in AddaVax and CpG+MPLA were different from the means of gene expressions in IVAX-1 (contrast test, with weights 1, 1, −1 respectively), using multcomp (v1.4.25).

CellChat analyses

To predict communication probabilities, CellChat (v1.6.1) was used.[24] We ran the pipeline with defaults up to calculating communication probabilities. We then calculated the synergy score of communication probabilities using the same formula as the synergy score of a gene:

$$synergy_p = log_2\left(\frac{mean(IVAX_p)}{mean(AddaVax_p) + mean(CpG+MPLA_p)}\right)$$

Where p is the probability of communication of a pathway.

Results

IVAX-1 combination adjuvant shows equivalent efficacy but improved viral clearance compared with emulsion or TLR agonists administered separately

Our previous studies using influenza HA H5 antigen showed that the magnitude and breadth of the antibody response induced by the squalene OW nanoemulsion, AddaVax, is enhanced by CpG and MPLA (TLR-9 and TLR-4 agonists,

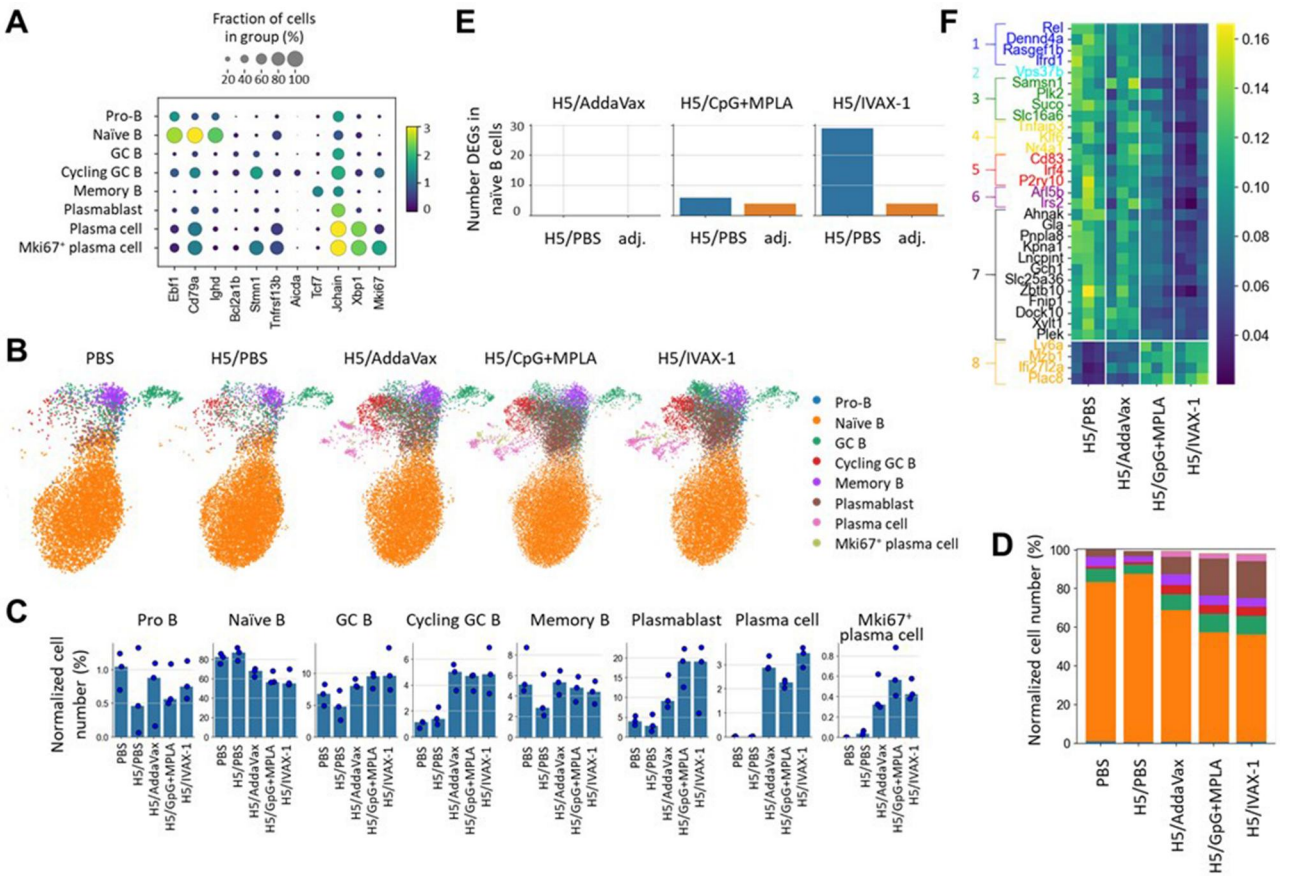

Figure 3. Analysis of B cells. (A) Bubble plot showing markers used to define B cell subsets, with shading and size of bubble representing mean expression in each group, and the proportion of each marker expressed in each B cell subset, respectively. (B) UMAPs of B cell subsets according to vaccine group. (C) Bar charts of normalized cell counts (expressed as % of total B cells) of each subset associated with each vaccine group; each dot represents an individual mouse. (D) Stacked plots of normalized cell counts shown in panel B, median of 3 mice. (E) Number of DEGs meeting cutoffs (Benjamini-Hochberg–corrected P values <0.2, log2 fold change >1) with log fold change higher in H5/PBS or adjuvanted formulations. Only naïve B cells in H5/CpG+MPLA and H5/IVAX had DEGs meeting the cutoff. See the main text for statistical test details. (F) Heatmap of the expression of the top DEGs in naïve B cells in IVAX/H5 vs PBS/H5. Downregulated gene groups correspond to genes related to NF-κB signaling (1), tumor suppressor (3), immune suppression (5), or combinations thereof (NF-κB and tumor suppressor (2), tumor suppressor and immune suppression (4), NF-κB and immune suppression (6), other down-regulated DEGs (black). Upregulated genes are group 8.

respectively), a combination adjuvant we have termed IVAX-1.[16] It is unknown, however, if the enhanced immunogenicity of IVAX-1 relative to its constituent components translates into enhanced efficacy against virus challenge in vivo. Therefore, we administered H5 in IVAX-1, or in either class of adjuvant separately (ie, H5/OW emulsion, and H5/TLR agonists) to groups of C57BL/6 female mice ($n = 10$ per group) via the subcutaneous (s.c.) route at the base of the tail (Fig. 1A). Control mice received either PBS, or H5 in PBS without adjuvants. Mice were boosted on day 28, and 3 mice were culled 4 d after the boost for single-cell mRNA sequencing of draining (inguinal) lymph nodes (Fig. 1B). The remaining 7 mice per group were challenged on day 96 with 10^4 $TCID_{50}$/mL H5N1 virus in a volume of 50 μL via the intranasal route. The magnitude of the H5-specific IgG response on day 14 (d14) (after prime only) revealed IVAX-1 generated the greatest magnitude and breadth, followed by CpG+MPLA, and finally by AddaVax. In the H5/PBS group, the response was not significantly different to PBS alone after a single dose (Fig. 1C) although signals of all 3 adjuvanted groups were high after boosting (Fig. 1C, inset). Th1/Th2 profiling on d42 postboost revealed a modest response by the H5/PBS group that was polarized entirely in an IgG1 (Th2) direction (Fig. 1D). The magnitude and breadth of this IgG1 response was significantly enhanced with AddaVax; this was also accompanied by the appearance of modest levels of IgG2c although the response was still overwhelmingly polarized to IgG1 (Th2). In contrast, mice receiving H5 in CpG+MPLA or CpG+MPLA+AddaVax (IVAX-1) produced a more IgG2c (Th1) skewed-response. Virus neutralization assays (Fig. 1E) revealed comparable nAb titers in all 3 adjuvanted groups, with no detectable neutralization in the PBS or H5/PBS control groups. Similarly, all 3 groups receiving adjuvanted H5 were equally well protected (100% survival) against H5N1 challenge, while control mice receiving PBS or H5/PBS were unprotected and were euthanized when they fell below 80% of their original body weight (Fig. 1F). Despite seeing no difference in nAb titers and efficacy when H5 was formulated in IVAX-1 compared with AddaVax or CpG+MPLA separately, we did observe a benefit on clearance of virus from the lungs from the

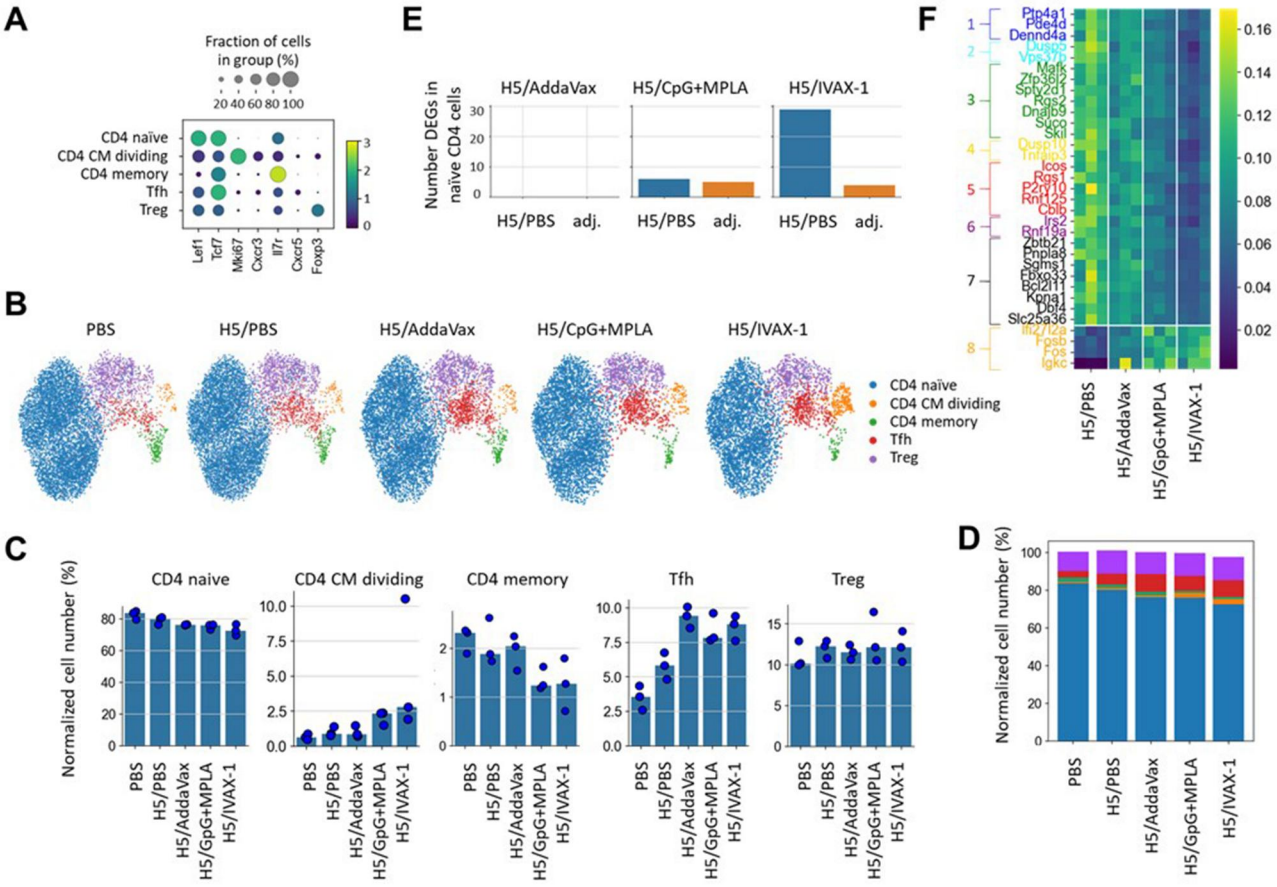

Figure 4. Analysis of CD4 T cells. (A) Bubble plot showing markers used to define CD4 T cell subsets, with shading and size of bubble representing mean gene expression in group and proportion of each marker expressed in each T cell subset, respectively. (B) UMAPs of CD4 T cell subsets according to vaccine group. (C) Bar charts of normalized cell counts (expressed as % of total CD4 cells) of each subset associated with each vaccine group; each spot represents an individual mouse. (D) Stacked plot of normalized cell counts as shown in panel B; median of 3 mice. (E) Number of DEGs meeting cutoffs (Benjamini-Hochberg–corrected *P* values <0.2, log2 fold change >1) with log fold change higher in H5/PBS or adjuvanted (adj.) formulations. Only the naïve CD4+ T cell population had DEGs meeting cutoff in CpG+MPLA and in IVAX compared with H5/PBS. (F) Heatmap of the expression of DEGs in naïve CD4 T cells in H5/IVAX compared with H5/PBS. Gene groups annotated as per Fig. 3.

IVAX-1 combination (Fig. 1G). Thus, the median titer on d6 in the H5/IVAX-1 group was ∼300-fold lower than the H5/CpG+MPLA, and ∼100-fold lower than H5/AddaVax.

Transcriptomic profiling 4 d after boost reveals increased proportions of B cells and monocytes with adjuvant complexity

To define the transcriptomic changes among different adjuvants, we sequenced 3 mice from each of the groups shown in Fig. 1A. Draining (inguinal) lymph nodes were collected 4 d after the boost and processed separately for single-cell RNA sequencing (10X Genomics; see Materials and Methods). We chose to perform single-cell RNA sequencing after the boost because we typically obtained several percent of antigen-specific T cells in recall assays by flow cytometry or ELISPOT. The day 4 time point was selected to capture the peak of activation and proliferation of responding lymphocyte (d3–5) before contracting.

After filtering cells based on the number of genes per cell, and genes based on the number of cells expressing that gene, we retained 146,532 cells by 21,822 genes. Genes used to identify major cell types are shown in Fig. 2A. The UMAP space is dominated by immune cells, which were classified by gene markers as B cells (*Cd79a*), plasma cells (*Cd79a* and *Sdc1*), T cells (*CD3e*), dendritic cells (*H2-Aa*), monocytes (*Lyz2*), and natural killer cells (*Ncr1*) (Fig. 2B). When UMAPs were plotted according to the vaccine groups (Fig. 2C), clear differences could be seen between the 2 non-adjuvanted groups (PBS and H5/PBS) and the 3 adjuvanted groups (H5/AddaVax, H5/CpG+MPLA) and H5/IVAX-1). To quantify this, the proportions of each cell type (medians of normalized cell numbers expressed as % of total cells) were plotted as separate bar charts to identify adjuvant effects within each cell type (Fig. 2D), and as stacked bar charts to assess adjuvant effects at the whole lymph node level. The proportions of B cell, plasma cells and monocytes increased with increased adjuvant complexity. The most dramatic effect was seen in plasma cells, with proportion means of 6.9%, 12.8%, and 12.1% for H5/AddaVax, H5/CpG+MPLA, and H5/IVAX-1, respectively, compared with 1.2% and 1.1% for PBS and H5/PBS, respectively. The

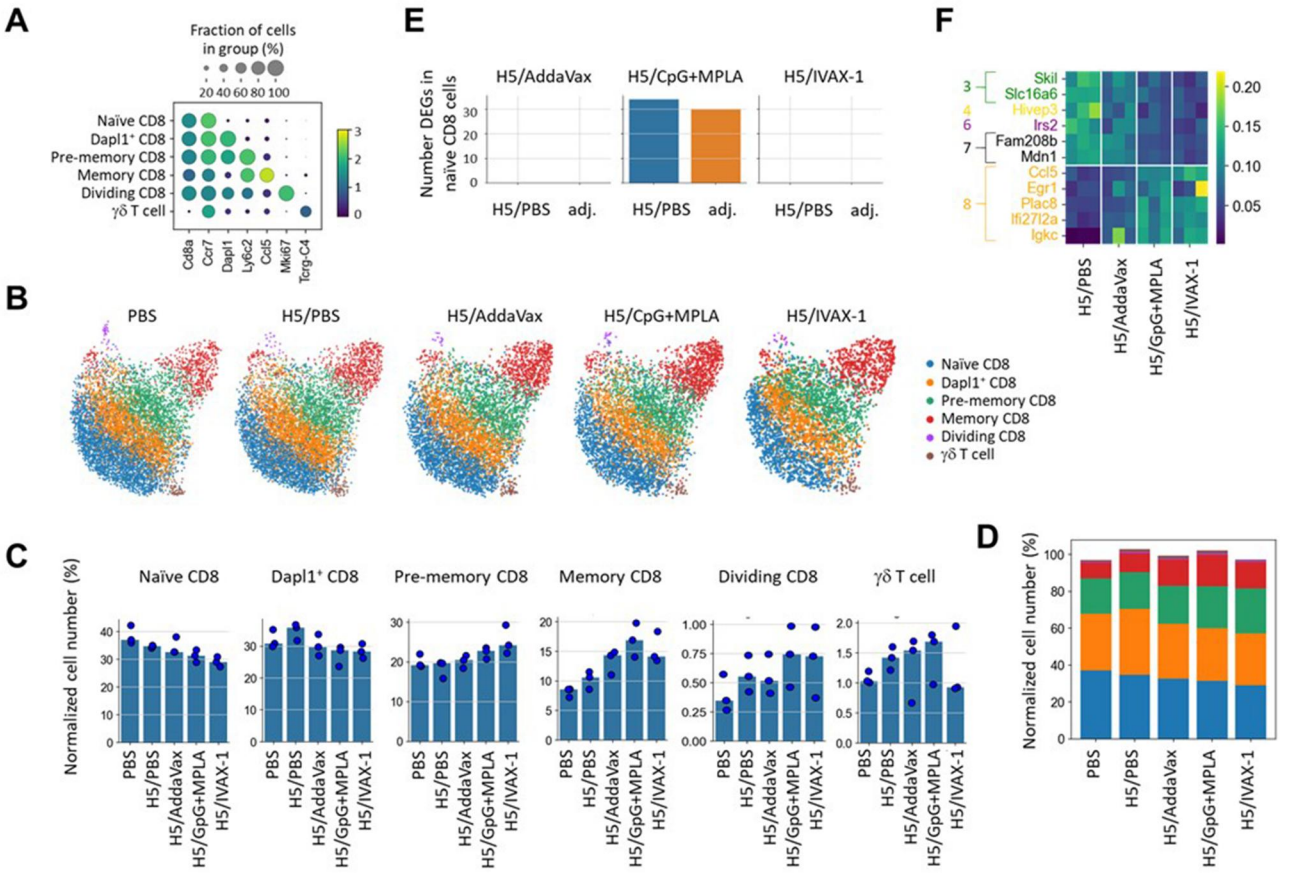

Figure 5. Analysis of CD8 T cells. (A) Bubble plot showing markers used to define CD8 T cell subsets, with shading and size of bubble representing gene expression level and proportion of each marker expressed in each T cell subset, respectively. (B) UMAPs of CD8 T cell subsets according to vaccine group. (C) Bar charts of normalized cell counts (expressed as % of total CD8 cells) of each subset associated with each vaccine group; each dot represents an individual mouse. (D) Stacked plot of normalized cell counts as shown in panel B, median of 3 mice. (E) Number of DEGs meeting cutoffs (Benjamini-Hochberg–corrected *P* values <0.2, log2 fold change >1) with log fold change higher in H5/PBS or adjuvanted formulations. Only the naïve, memory, prememory, and Dapl1+ CD8 T cell populations had DEGs meeting cutoff in H5/CpG+MPLA compared with H5/PBS; (F) Heatmap of the expression of the DEGs in naïve CD8 T cells in H5/CpG+MPLA versus H5/PBS.Gene groups annotated as per Fig. 3.

proportions of T and natural killer cells decreased with increasing adjuvant complexity, owing to the expansion of B and plasma cells, while the proportion of dendritic cells stayed relatively stable. Overall, the effects of H5/CpG+MPLA and H5/AddaVax+CpG+MPLA (IVAX-1) were more similar to each other than to H5/AddaVax, while all 3 adjuvanted groups were more similar to each other than the nonadjuvanted (PBS and H5/PBS) groups. The following sections describe adjuvant effects on the main lymphocyte subsets in more detail.

Adjuvants enhance numbers of germinal center B cells and plasma cells

We first characterized B cells in the dataset. The gene markers used to define different B cell subsets are shown in Fig. 3A. The gene marker *Cd79a* was used to define all B cells, and subsets thereof were defined as pro–B cells (*Ebf1*),[25] naïve B cells (*Ighd*),[21] light zone cells (*Bcl2a1b*),[21] dark zone cells (*Stmn1*),[21] a population of germinal center (GC) B cells (*Stmn1*, *Tnfrsf13b*, and *Aicda*),[21] cycling GC B cells (*Aicda* and *Mki67*),[21,26] and memory B cells (*Tcf7*).[21] The plasma cells were composed of plasmablasts (*Jchain*),[21] plasma cells (*Jchain* and *Xbp1*),[21] and dividing plasma cells (*Xbp1* and *Mki67*).[21,26]

UMAP plots of these subsets according to vaccine group are shown in Fig. 3B, which shows discernable expansion of several B cell subsets associated with the adjuvants, particularly plasma cells and plasmablasts. To quantify these adjuvant effects, the proportions of each subset (expressed as % of all B cells) was defined and represented as bar plots (Fig. 3C) and as a stacked plot (Fig. 3D). The proportions of GCs, cycling GCs and all plasma cell subsets all increased with adjuvant complexity, while there were no discernable changes in the proportions of pro–B cells or memory B cells. The proportion of naïve B cells decreased from nonadjuvanted to adjuvanted conditions. These data reflect a progressively increasing effect of adjuvant complexity on antibody-secreting B cells.

We also calculated the pseudotime trajectories for the B cell populations, along with DEGs along the trajectory (Fig. S1). There were several immediate early genes (*Egr1*, *Fosb*, *Jun*, *Fos*, *Junb*) with high expression in naïve B cells that decreased along the trajectory, along with *Ebf1*, known to be a crucial gene in B cell development and maintenance,[25] as well as *H2-Ab1* and *Cd74* involved in antigen presentation to T cells.[27]

We next determined the number of DEGs between each of the 3 adjuvanted formulations and the H5/PBS control in each B cell subset. We leveraged the number of batches per group by pseudobulking each batch, normalizing by total counts, and using MWU for hypothesis testing (see Materials and Methods). Only naïve B cells showed any differential expression at this time point (4 d postboost), and differences were confined to the H5/CpG+MPLA and H5/IVAX-1 groups (Fig. 3E). The detection of DEGs in naive B cells only may reflect their being in the early stages of differentiation, although this may also be caused by the relative abundance of naive B cells, thereby facilitating the statistical detection of DEGs in this group. Relatively few genes were upregulated (Fig. 3F); these had disparate functions and comprised *Mzb1* (marginal zone B and B1 cell–specific protein), *Ifi27l2a* (interferon, alpha-inducible protein 27 like 2A), *Ly6a* (lymphocyte activation protein-6A), and *PLAC8* (placenta associated 8). *Mzb1* is constitutively expressed in innate-like B cells (marginal zone B cells, B1 cells) and is significantly upregulated in plasma cells, where it functions as a molecular chaperone to facilitate assembly of IgA and IgM with J-chain and transcytosis into mucosal secretions.[28,29] *Ifi27l2a* is an antiviral interferon-response gene that is upregulated in several cell types in response to infections, including lung macrophages and lymphocytes,[30] microglia [31,32] and mucosal epithelium.[33] Our results indicate that *Ifi27l2a* is also upregulated by IVAX-1, predominantly by the TLR4 and/or TLR9 agonist components. The *Ly6a* gene product is upregulated on activated lymphocytes although its function remains unclear.[34] Similarly, PLAC8, first discovered in a placenta expression library,[35] plays a role in T cell immunity (see the following), although its role in B cells is unknown.

In contrast, many more genes were downregulated relative to the control, with log2 fold changes <−11 (Fig. 3F). Of these, 7 were linked to NF-κB signaling, namely *Ifrd1*,[36,37] *Rasgef1b*,[38] *Dennd4a*,[39] *Rel*,[40] *Vps37b*,[41] *Irs2*,[42,43] and *Arl5b*[39,44]; 7 genes were directly or indirectly identified as tumor suppressor genes (TSGs), namely *Vps37b*,[41] *Plk2*,[45] *Suco*,[46] *Samsn1*,[47] *Tnfaip3*,[48] *Klf6*,[49] and *Nr4a1*[50,51]; and 8 genes were linked to immune suppression, including *Tnfaip3*,[48,52] *Klf6*,[49] *Nr4a1*,[50,51] *Cd83*,[51,53,54] *P2ry10*,[55] *Irf4*,[56] *Irs2*,[42,43] and *Arl5b*.[39,44] These results imply that the adjuvants greatly increase the proportions of GCs and plasma cells and decrease the proportion of naïve B cells, suggesting an activation of naïve B cells transitioning toward a differentiated plasma cell state. This cell state transition is also correlated with downregulation of immune homeostasis and TSGs, consistent with entry into cell cycle.

Adjuvants expand T follicular helper cells

We next defined CD4 T cell subsets. CD4 T cells were defined by expression of the *Cd4* gene, with 5 subsets identified: naïve CD4 T cells, *Lef1*[57] and *Tcf7*[58] expression; dividing CD4 central memory (CM) T cells, *Mki67*[26] and *Cxcr3*[59]; CD4 memory T cells, *Il7r*[60]; T follicular helper T (Tfh) cells, *Cxcr5*[61]; and T regulatory (Treg) cells, *Foxp3* (Fig. 4A).[62,63] UMAPs according to vaccine groups (Fig. 4B) show discernible expansion of Tfh cells. Proportions of each subset (expressed as % of all CD4 T cells) were determined and represented as bar plots (Fig. 4C) and a stacked plot (Fig. 4D). There was a small yet significant decrease of naïve $CD4^+$ T cells associated with adjuvanted H5 versus H5/PBS (P value = 0.036, MWU) and an increase of Tfh cells associated with adjuvant (P value = 0.009, MWU). There was no significant change in the proportion of dividing CM CD4 T cells, memory CD4 T cells, or Treg cells in adjuvanted H5 groups combined versus H5/PBS (P values of 0.145, 0.145, and 0.727, respectively, MWU). However, the proportion of dividing CM cells did significantly increase when H5/CpG+MPLA and H5/IVAX-1 were compared separately to H5/PBS (P values of 0.1 and 0.1, respectively, MWU), and there was a significant decrease of memory CD4+ T cells in H5/CpG+MPLA (P value of 0.1). Overall, the expansion of Tfh cells and dividing CM cells are consistent with the increase in plasma cells and plasmablasts seen previously.

We further characterized the $CD4^+$ T cell population by calculating their pseudotime trajectories (computationally inferred differentiation trajectory) along with DEGs along this trajectory. We used the same principal components used to calculate the UMAPs in Fig. 4 but allowed the UMAP to be recalculated to optimize the trajectory projection onto 2 dimensions (see Methods). The naïve CD4 T cell population was totally disconnected from the other populations, implying that the naïve population is more different to the other populations than the other populations are to themselves (Fig. S2). The DEGs along the pseudotime trajectory include Treg marker genes; *Foxp3*,[62,63] *Il2ra* and *Il2rb*[64]; 2 S100 family genes, *S100a4* and *S100a6*; and *Cxcr6*, which has been shown to be important for T cell recruitment.[65,66]

Finally, we characterized the DEGs (using the same pseudobulking and MWU procedure as previous) between the PBS/H5 formulation and the 3 adjuvanted formulations. As with B cells, only the naïve T cells in the H5/CpG+MPLA and H5/IVAX groups had DEGs after filtering based on cutoffs (log2 fold change >1, false discovery rate–adjusted P value <0.2) (Fig. 4E). Relatively few genes were upregulated. As seen with B cells, these included *Ifi27l2a*, an interferon-response gene that is upregulated in several cell types in response to infections; *Fos* and *Fosb*, both components of the AP-1 transcription factor that regulates cell proliferation and differentiation in the immune response;[54,67] and *Igkc*, the κ chain of immunoglobulin with no known function in T cells.

As with B cells, many more genes were downregulated genes in the naïve T cell population at this time point (Fig. 4F), which included 7 NF-κB–related genes, namely *Pde4d*,[68] *Dennd4a*,[39] *Ptp4a1*,[69] *Vps37b*,[41] *Dusp5*,[70,71] *Irs2*,[42,43] and *Rnf19a*[72]; 11 TSGs, namely *Vps37b*,[73] *Dusp5*,[70,71] *Mafk*,[74] *Dnajb9*,[75] *Suco*,[46] *Spty2d1*,[76] *Rgs2*,[77] *Zfp36l2*,[78] *Dusp10*,[79,80] *Tnfaip3*,[48,81] and *Skil*[82]; and 9 immune suppression genes, namely *Dusp10*,[79,80] *Tnfaip3*,[48,52,83] *Rgs1*,[84] *P2ry10*,[55] *Cblb*,[85] *Rnf125* (*TRAC-1*),[86,87] *Icos*,[88] *Irs2*,[89] and *Rnf19a*.[72] These results indicate that, similarly to B cells, naïve CD4 T cells downregulate immune homeostasis genes.

Adjuvants reduced the proportion of naive CD8 T cells

We then characterized CD8 T cell subsets. After unsupervised clustering, we found 5 groups of cells (Fig. 5A): naïve CD8 T cells, *Ccr7*[90] expression; memory CD8 T cells, *Ccl5*,[91] and dividing CD8 T cells, *Mki67*; *Dapl1* CD8 T cell subset,[92] and a *Ly6c2*[92] *Ccl5*-expressing subset,. which we labeled "prememory" CD8 T cells. To validate this subset further, DEGs between the prememory and memory $CD8^+$ T cells were determined (Fig. S3). Of note, *Ccr7* is more highly expressed in prememory $CD8^+$ T cells, whereas memory T cells

have higher expression of *Ccl5* and IL-18 (*Ifng*, *Pdgfb*, and *Il18rap*) and Ly49 family (*Klra1*, *Klre1*, *Klra6*, and *Klra9*) genes, further validating the classification of this CD8$^+$ T cell subset.[93] We also identified a cluster of γδ T cells (*Tcrg-C4*) which we placed into the dividing CD8 T cell subset for convenience.

UMAP plots for each vaccine group are shown in Fig. 5B. Proportions of each subset (expressed as % of all CD8 T cells) were determined and represented as bar plots (Fig. 5C) and a stacked plot (Fig. 5D). As with the CD4 T cells, the naive CD8 T cells were the greatest proportion of all CD8 T cells, and showed a small yet significant decrease with addition of adjuvant versus H5/PBS (P value = 0.06, MWU). The prememory and memory subsets increased with adjuvants; the Dapl1+, dividing CD8 T cells and γδ T cells stayed constant.

We also calculated the pseudotime trajectories of the CD8$^+$ T cells, with the differential expression along this trajectory. Most of the DEGs along the pseudotime trajectory match the marker genes previously identified, except for *Samd3* which has been recently discovered to be a memory CD8 T cell marker of unknown function,[94] and *Klf2* which is known to suppress T cell maturation and activation in naïve T cells (Fig. S4).[95,96]

We calculated the DEGs in the 3 adjuvanted groups combined versus H5/PBS using the method described previously (Fig. 5D). Unlike in the preceding analyses, only T cells in the H5/CpG+MPLA adjuvanted group had DEGs. We selected the naïve CD8 T cells for further analysis (Fig. 5E). The 5 upregulated genes comprised *Ifi27l2a* (also seen upregulated in B cells and CD4 T cells described previously), *Ccl5*, *Egr1*, *Plac8*, and *Igkc*. *Ccl5* (RANTES) is a T cell chemoattractant/chemokine required for T cell migration and homing to sites of infection[97]; *Egr1* (early growth response-1) is a transcriptional regulator required for cell proliferation and differentiation[98]; *Plac8* is reported to be expressed in Th1 CD4 cells, where it suppresses expression of IFNγ[99]; andthe same study also reported expression in CD8 and promotes establishment of influenza-specific CD8 T cells in vivo.[99] *Igkc*, the kappa chain of Ig, is also upregulated in CD4 T cells but has no known function in CD4 or CD8 cells and may not be translated. Of the 5 genes downregulated in mice receiving H5/CpG+MPLA compared with H5/PBS, 3 have been linked to tumor suppression, *Skil*,[82] *Slc16a6* [100] and *Hivep3*[101]; 2 have been linked to immune suppression; *Hivep3*[102] and *Irs2*[89]; and 1 was linked to NF-κB signaling, *Irs2*.[42,43] *Irs2* mediates Th2 signaling and macrophage activation via the type I IL-4 receptor.[98,99]

Overall, the data show that the adjuvants examined cause a strong downregulation in naïve T and B cells of genes that have been previously tied to immune suppression or immune homeostasis, tumor suppression (which could equivalently be called proliferation suppression) and NF-κB signaling, which is canonically tied to immune activation and differentiation.[103] We propose that these genes normally maintain a state-immune homeostasis in the adaptive immune system, but which are downregulated in naive lymphocytes by adjuvants, thereby releasing the brakes on cell cycle and allowing naïve lymphocytes to reach a poised state undergo proliferation and differentiation into effector cells upon antigen encounter.

IVAX-1 confers synergistic effects on immune hemostasis genes

The immunological studies described previously showed that administration of H5 in the combination of CpG+MPLA with AddaVax (IVAX-1) synergistically enhanced viral clearance from lungs (Fig. 1E) compared with administration of H5 in CpG+MPLA or AddaVax separately. Therefore, we assessed whether the IVAX-1 combination adjuvant also showed any synergistic effects at the transcriptomic level, particularly in the downregulation of the immune homeostasis genes. We define synergy as "more than additive," meaning that the sum of the mean of transcriptomic expression of IVAX-1 is greater than the sums of the means of transcriptomic expression in the AddaVax and CpG+MPLA groups separately (see Materials and Methods). A synergy score <0 implies smaller than additive expression in IVAX-1. In order to account for random fluctuations between groups, we fit a linear model to the pseudobulked transcriptomic expression of each cell state with covariate formulation, and calculated the P value of the linear combination of coefficients corresponding to our definition of synergy (see Materials and Methods for details).

Figure 6A shows an overall heat map of immune homeostasis gene expression in the naïve CD4, naïve CD8, and naïve B cells, ranked top to bottom within each cell type by increasing adjuvant complexity. It can be seen that for many genes there is decrease in expression, as described in the preceding sections. Synergy scores are shown in Fig. 6B. Surprisingly, with one exception, all the genes we categorized as immune homeostasis genes had a synergy P value of <0.05 and a synergy score <−1; the exception was *Icos* in naïve B cells, with a P value = 0.1 and a synergy score of −0.75. This implies that for almost all identified immune homeostasis genes in naïve CD4 T, CD8, and B cells, IVAX-1 had at least a log2 fold change, equivalent to a 2-fold downregulation, compared with the additive prediction of AddaVax and CpG+MPLA separately.

In addition to synergistic expression of genes, we also compared the strength of cell-cell signaling between cell subsets using CellChat.[24] We first computed the differential interaction strength for each vaccine formulation compared with H5/PBS, where blue edges indicate higher expression in H5/PBS, and red edges indicate higher expression in the other conditions (Fig. 6C). Overall, there was higher signaling in the adjuvanted conditions compared with H5/PBS, with most differential signaling going toward CD8 T cells. We then calculated the synergistic signaling in IVAX-1 compared with AddaVax and CpG+MPLA using the same procedure as previous, by simply replacing expression values with communication probabilities, and keeping the same thresholds (see Materials and Methods). As before, we focused on downregulated synergistic probabilities. The number of synergistic communications in each source/target pair are shown in Fig. 6D. The majority senders of synergistic communication were naïve B cells, CD4 CM dividing T cells, and dividing CD8 T cells. The majority of receivers were memory CD8 T cells, CD4 CM dividing T cells, Treg cells, and CD4+ naïve T cells. Among the most active interactions were between naive B cells signaling to CD4 CM dividing T cells and Treg cells, presumably reflecting presentation of antigen by B cells in the context of class II major histocompatibility complex (MHC) to both CD4 T cell subsets. Similarly, CD4 CM dividing T cells were actively signaling to prememory and memory CD8 T cells, consistent with a role for CD4 CM T cells in the development of CD8 T cell memory.[106] Given the large differences found previously within naïve B cells, and the importance of Treg cells in preventing overactivation of an immune response, we further analyzed the signaling from naïve B cells to Treg cells (Fig. 6E). Interestingly, we saw synergistic

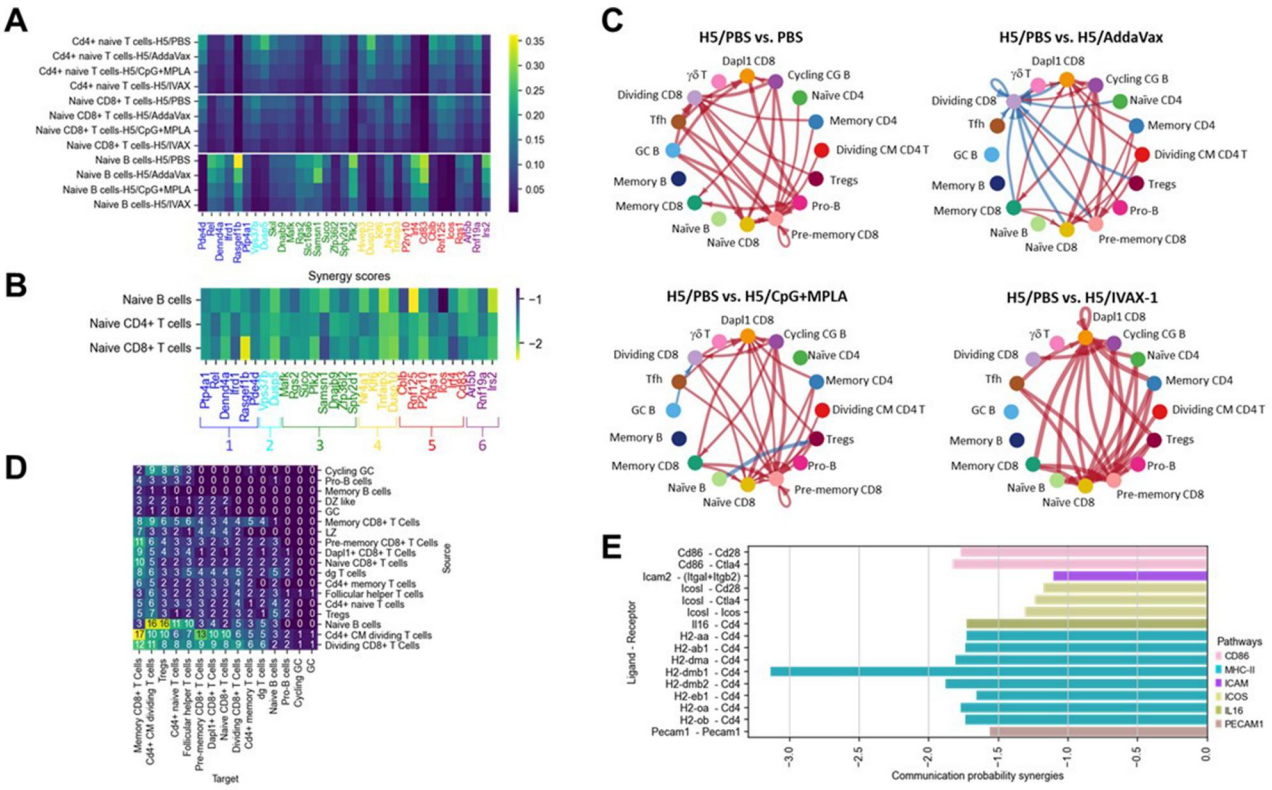

Figure 6. IVAX induces synergistic downregulation of both immune homeostasis genes and immune suppressive signaling. (A) Psuedobulked expression of naïve CD4 and CD8 T cells, and naïve B cells of immune homeostasis genes (see main text). (B) Synergy scores for immune homeostasis genes (logged quotient of IVAX-1 expression to the sum of CpG+MPLA and AddaVax expression separately, in which a score of <−1 implies synergistic effect; see main text for details); gene groups annotated as per Fig. 3. (C) Cumulative strength of T and B cell signaling in the H5/PBS group versus other groups; the width of edges indicates the strength of signaling. (D) The number of synergistic signaling pathways in each source/target pair of different cell types. (E) The synergistic signaling pathways along with signaling synergy score (calculated the same as synergy score, see the main text) from naïve B cells to Treg cells.

downregulation of genes of several ligand/receptor pairs, including the costimulatory interaction between *Cd86* and *Cd28*, and the T cell inhibitory interaction between *Cd86* and *Ctla4*. Synergistic downregulation of the interaction between *Cd4* and several genes encoded in class II region of the MHC in Treg cells were also observed, consistent with the antigen-presenting role of B cells speculated previously. We also observed downregulation of the *Cd4* gene in Treg cells, which led to a downregulation of signaling of MHC class II genes to this coreceptor (Fig. 6E). Rapid downregulation of surface CD4 is known to occur after T cell receptor–mediated activation,[104–106] and may serve to transiently desensitize T cells. The downregulation of *Cd4* expression in Treg cells would be consistent with detuning of Treg cells to allow an immune response to occur.

IVAX-1 enhances efficacy after single-dose administration

Given the transcriptomic evidence of the synergistic effects of combining CpG+MPLA with AddaVax emulsion, we sought to find other benefits of combining the adjuvants at the in vivo level. For this, we performed antigen dose-sparing and single-dose vaccination studies. Groups of 5 mice were administered 5 μg or 1 μg H5 in IVAX-1, AddaVax, or CpG+MPLA in a prime/boost regimen, or 5 μg H5 adjuvanted in the same way but administered as a single-dose only. Mice receiving H5/PBS were used as challenge controls. Comparable levels of survival were achieved at both the 5 μg and 1 μg H5 doses using all 3 adjuvant formulations after a prime and boost (data not shown). However, a clear benefit of IVAX-1 over AddaVax or CpG+MPLA used separately was revealed after single-dose administration (Fig. 7A). Thus, mice primed with H5/IVAX-1 were protected against mortality (100% survival), while mice receiving a single dose of H5/AddaVax or H5/CpG+MPLA were either unprotected (0% survival) or partially protected (40% survival), respectively. IgG subtyping (Fig. 7B) revealed a similar pattern to that seen with the prime-boost regimen, characterized by a strongly polarized Th2/IgG1 response by antigen alone or in emulsion, which becomes more skewed toward a Th1/IgG2c with the addition of CpG+MPLA. AddaVax enhances the magnitude and breadth of the response seen by antigen alone or antigen/CpG+MPLA. These indicate the lack of efficacy from a single dose of H5 in AddaVax or CpG+MPLA was not caused by a shift in Th1/Th2 balance. Adjuvants that allow for single-dose vaccination may have applications in influenza pandemics in which vaccine supplies are limited, or in which rapid acquisition of immunity is desirable.

Discussion

The formulation of IVAX-1 studied here was selected on the basis of previous immunogenicity screens with influenza and Ebola virus surface antigens in mice with different TLR agonists administered with or without AddaVax emulsion.[16,17]

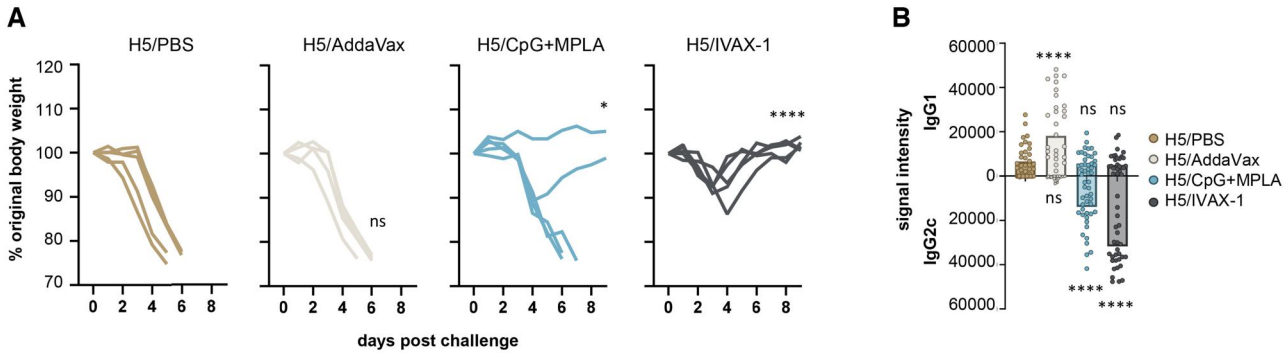

Figure 7. IVAX-1 shows efficacy from a single dose. Groups of 5 C57BL/6 female mice were administered 5 μg H5 (VN04) formulated in PBS, AddaVax, CpG+MPLA, or IVAX-1 on d0 via the subcutaneous route and challenged on d28 with 50 μL 10^4 $TCID_{50}$ /ml of H5N1 virus. (A) normalized body weights postchallenge; each line represents an individual mouse. (B) IgG1/IgG2c (Th2/Th1) profiles on d23 determined by protein microarray, in which each spot is a different H5 drift variant. Two-way analysis of variance between H5/PBS and other groups; Dunnett's multiple comparisons test. $*P < 0.05$; $****P < 0.0001$. ns, nonsignificant.

These studies showed IVAX-1 consistently outperformed the individual components in immunogenicity studies. Hitherto, however, we had not reported on efficacy in challenge studies. Contrary to expectations, H5 administered in IVAX-1, CpG+MPLA, or AddaVax all engendered comparable levels of H5N1 nAbs and efficacy against weight loss after H5N1 challenge (Figs. 1E and F), despite IVAX-1 being more immunogenic in our prior studies. Given that adjuvants have the potential to cause undesirable side effects,[107] it is important to justify their inclusion when used in combination. In this regard, the IVAX-1 combination did result in 100- to 300-fold less virus in the lungs on d6 postchallenge than CpG+MPLA or AddaVax administered separately (Fig. 1G), indicating a synergistic effect on viral clearance. We also observed a similar synergistic clearance of SARS-CoV-2 from the lungs of hamsters administered Spike protein in IVAX-1 compared with administration in either AddaVax or CpG+MPLA alone (manuscript in preparation). We also noted that nAb titers achieved from AddaVax, CpG+MPLA and IVAX-1 were equivalent, while a nonfunctional binding assay (protein microarray) revealed higher signals associated with IVAX-1 and CpG+MPLA compared with AddaVax. The role of nonneutralizing antibodies is presently unclear, but these may contribute to protection by other means such as opsonization and enhanced antigen presentation, complement fixation, or antibody-dependent cell-mediated cytotoxicity.

An additional benefit of IVAX-1 versus the individual components was revealed after single-dose administration (Fig. 7). Single-dose vaccines may have utility in pandemic situations where rapid responses are essential, or in settings where vaccine supplies are limited. Traditionally, durable immunity from single-dose vaccination has best been accomplished using live/attenuated vaccines, notably vaccinia (smallpox vaccine) [108] and yellow fever (YF) vaccine.[109] The YF vaccine is probably the most effective of all live vaccines, being able to confer durable immunity from a single dose in nearly all vaccinated individuals.[109,110] Systems immunology approaches have revealed YF induces a panoply of innate and adaptive immune responses, spanning complement, type I interferons, inflammasomes, and rapid T and B cell responses.[111–113] For nonlive (ie, recombinant protein based) vaccines, priming followed by 1 or more boosts are typically required to drive the germinal center reaction and generate protective titers of neutralizing antibodies.[113,114] Attempts to enhance the efficacy from single-dose vaccination have typically used controlled-release strategies in place of traditional bolus immunizations, which are thought to more closely mimic natural infection.[115–117] However, adequate protection can also be achieved from a single dose of recombinant protein by the use of certain adjuvants.[118–120] In practice, there may be several strategies that could achieve protection from single-doses of nonlive vaccines. The mechanism of protection achieved from a single-dose of IVAX-1 is not yet understood but is likely to be independent of nAbs, because in our experience the generation of nAbs typically requires boosting.[16,20]

Transcriptomic analyses of immune cells in draining lymph nodes 4 d postboost were used to compare IVAX-1 with CpG+MPLA or AdaVax separately, and with nonadjuvanted controls for signs of additive or synergistic responses. We observed a dramatic increase in plasma cells after H5 administration in IVAX-1, which was ~2-fold higher than administration in CpG+MPLA or AddaVax, and ~10-fold higher than antigen administered without adjuvant. However, unbiased DEG screens comparing unadjuvanted H5 with the adjuvanted groups at d4 postboost revealed relatively few genes that were upregulated. Of note, *Mzb1* expression in B cells is higher in response to IVAX-1 and CpG+MPLA compared with AddaVax. Given the role of *Mzb1* in the assembly of IgA and IgM with J-chain and transcytosis into mucosal secretions,[28,29] biochemical studies to confirm enhanced protein expression are warranted, as this would be consistent with the synergistic clearance of virus from lungs achieved by the IVAX-1 combination. Unbiased DEG screens in T cells also revealed relatively few genes were upregulated but included adjuvant-dependent expression of *Fos*, *Fosb*, *Ifi27l2a*, and *Igkc* (CD4 cells) and *Ccl5*, *Egr1*, *Plac8*, *Ifi27l2a*, and *Igkc* (CD8 cells). Targeted (biased) screens of the CD4 T cell compartment revealed upregulation of PD-1 (*Pdcd-1*) in Tfh cells and dividing CD8 T cells, which was also higher in mice receiving H5/IVAX-1 than the individual components. PD-1 induces a co-inhibitory signal in activated T cells and promotes T cell apoptosis, anergy, and functional exhaustion[121,122] and is likely to be involved here in the downregulation of T cells at d4 postboost. Other lymphoid cell markers were not elevated at this time point.

In contrast, DEG screens revealed many more downregulated genes compared with upregulated genes. In all the cell types examined, there was a clear correlation between downregulation of genes that control cell cycle/apoptosis and

adjuvant complexity, consistent with a role for adjuvants in releasing the brakes on immune-homeostasis and driving the immune response. For example, in B cells, adjuvant-dependent downregulated genes include the TSGs *Vps37b*,[41] *Plk2*,[45] *Suco*,[46] *Samsn1*,[47] *Klf6*,[49] *Nr4a1*,[4,51] and *Tnfaip3* (Fig. 3F).[48] Those with a putative role in B cell function include *Vps37b* (vacuolar protein sorting 37 b), which not only is normally involved in transport vesicle sorting, possibly in B cells for antigen processing,[123] but also is downregulated in colorectal cancers[41]; *Plk2* (Polo-like kinase 2) is a serine/threonine kinase normally involved in B cell activation, but defects in this gene are associated with B cell malignancies[45]; *Samsn1* (SAM domain, SH3 domain and nuclear localization signal 1) encodes a cytoskeletal protein that is normally a negative regulator of B cell activation,[124] but which is overexpressed in malignant plasma cells[125]; *Nr4a* receptors restrain B cell responses to antigen in the absence of costimulation[126]; and *Tnfaip3* (TNF-α induced protein 3, formerly known as A20) is a cytokine-inducible gene that negatively regulates NF-κB and inhibits apoptosis.[83] Defects in this gene in B cells lead to enhanced inflammation and autoimmune disease.[127,128]

In T cells, adjuvant-dependent downregulated genes include 11 TSGs. Those with putative roles in T cell function include *Vps37b*, a memory T cell marker[129]; *Dusp5*, which promotes T cell survival[130]; *Rgs2* (regulator of G protein signaling 2), which controls T cell proliferation and IL-2 production in T cells[131]; *Zfp36l2*, which regulates T cell immune homeostasis[132]; *Dusp10*, which is constitutively expressed in T cells but downregulated after activation[133]; and *Tnfaip3*, an NF-κB inhibitor that is expressed at high levels in resting T-cells[134] but is degraded after T cell activation to facilitate NF-κB translocation.[135]

Genes linked to immune suppression are also downregulated. In B cells these include *Tnfaip3*,[48,52] *Klf6*,[49] *Nr4a1*,[50,51] *Cd83*,[53,54] *P2ry10*,[55] *Irf4*,[56] *Irs2*,[42,43] and *Arl5b*.[39,44] In addition to those discussed previously are *Cd83*, which is associated with a shift to a Th2 response and secretion IgE when downregulated in B cells[53]; *Irf4* (interferon regulatory factor 4), which is involved in B cell differentiation[86]; and *Irs2* (insulin receptor substrate 2), which is involved downstream of B cell receptor–initiated signaling and plays a role in B cell immune homeostasis.[42] In T cells, downregulated immune suppression genes include *Dusp10*,[79,80] *Tnfaip3*,[48,52,83] *Rgs1*,[84] *P2ry10*,[55] *Cblb*,[85] *Rnf125* (*TRAC-1*),[136,137] *Icos*,[88] *Irs2*,[89] and *Rnf19a*.[72] In addition to those discussed previously, those with a putative role in T cell function include *Rgs1*, which regulates tissue resident memory T cells[87] and T cell exhaustion[138]; *P2ry10*, which regulates chemokine-induced migration of T cells[139]; *Cblb*, which plays critical roles in T cell activation and homeostasis[140]; *Rnf125*, a regulator of T cell activation[136,137]; *Icos*, which regulates T cell activation and proliferation[88]; and *Irs2*, which is involved in signaling triggered by the IL-4 receptor on Th2 cells.[141]

Although the role that dysregulation of TSGs have in oncogenesis has long been recognized, their role in immune regulation has become evident only recently.[142] For example, p53 is a master regulatory transcription factor that normally controls entry into cell cycle, DNA repair, and apoptosis, and many tumors are associated with mutated or deleted p53.[143] In addition, p53 is thought to play a role in the control of various viral pathogens.[144] For example, in influenza, mice deleted of p53 show more severe disease compared with wild-type mice, with delayed cytokine and antiviral gene expression, reduced dendritic cell activation, and impaired CD8 T cell responses.[145] The importance of p53 in antiviral immunity is also evidenced by the strategies that some viruses have evolved to subvert its activities.[146] Given our findings, it is not surprising that vaccine adjuvants, which are designed to activate the innate immune system through recognition of pathogen-associated molecular patterns, may act to switch off TSGs and other genes that maintain immune homeostasis. As far as we are aware, the downregulation of immunosuppressive and TSGs by vaccines is not widely reported.[147] Indeed, downregulation of immune homeostasis genes, such as by using combination adjuvants, might represent an additional strategy to improve the efficacy and durability of subunit vaccines.

Transcriptomic studies provide comprehensive data on gene expression but not translated protein expression levels or activities. Such observations need to be followed up with biochemical or immunological studies. Other limitations of the present study include the single time point used for single-cell mRNA sequencing. This provides a snapshot, rather than a temporal pattern of expression, and significant genes that peak at earlier or later time points will be missed. Selection of the time point was informed by our previous studies of where numbers of antigen-specific B cells were quantified by flow cytometry.[16,20] Another limitation may have been the dose of adjuvants that were used, which may have been too high, as the efficacy against H5N1 challenge of IVAX-1 was the same as the AddaVax and CpG+MPLA administered separately. The advantages of combining adjuvants may be observed only at more stringent conditions, such as lower doses of adjuvant and/or antigen, or after single-dose administration, or in challenge studies against HA variants outside the vaccine formulation.

In summary, both immunological and transcriptomic data show benefits of combining TLR-agonists (CpG and MPLA) with the squalene-in-water emulsion, AddaVax compared with the CpG+MPLA or AddaVax alone. In particular we noted improved downregulation of immune hemostasis pathways, higher numbers of plasmablasts and enhanced viral clearance. Combination adjuvants, such as IVAX-1, may lead to the development of improved vaccines for single-dose or dose-sparing applications, and may also enhance the efficacy of vaccines against respiratory viruses.

Acknowledgments

The authors thank Suhas Sureshchandra and Lisa Wagar (University of California, Irvine Department Physiology and Biophysics) for stimulating discussions.

Supplementary material

Supplementary material is available at *ImmunoHorizons* online.

Funding

This work was supported by National Institutes of Health (NIH)/National Institute of Allergy and Infectious Diseases (NIAID) Molecular Mechanisms of Combination Adjuvants (MMCA) program, grant U01AI160397 (D.H.D.), Defense Threat Reduction Agency (DTRA) grant HDTRA-1-18-0036

(D.H.D.), NIH/NIAID grant R01AI168063 (S.O.), National Science Foundation (NSF) grant DMS1763272 (Q.N.), and a grant from the Simons Foundation (594598 [Q.N.]). This work utilized resources of the University of California, Irvine (UCI) Genomics Research and Technology Hub, parts of which are supported by NIH grants to the Comprehensive Cancer Center (P30CA-062203) and the UCI Skin Biology Resource Based Center (P30AR075047) at the UCI, as well as to the Genomics Research and Technology Hub for instrumentation (1S10OD010794-01 and 1S10OD021718-01).

Conflicts of interest

None declared.

Data availability

Protein microarray and/or single cell mRNA seq data underlying this article will be shared on reasonable request to the corresponding author.

References

1. Singleton KL, Joffe A, Leitner WW. Review: current trends, challenges, and success stories in adjuvant research. Front Immunol. 2023;14:1105655.
2. Firdaus FZ, Skwarczynski M, Toth I. Developments in vaccine adjuvants. Methods Mol Biol. 2022;2412:145–178. https://doi.org/10.1007/978-1-0716-1892-9_8.
3. Raponi A, Brewer JM, Garside P, Laera D. Nanoalum adjuvanted vaccines: small details make a big difference. Semin Immunol. 2021;56:101544. https://doi.org/10.1016/j.smim.2021.101544.
4. He P, Zou Y, Hu Z. Advances in aluminum hydroxide-based adjuvant research and its mechanism. Hum Vaccin Immunother. 2015;11:477–488. https://doi.org/10.1080/21645515.2014.1004026.
5. Del Giudice G, Rappuoli R, Didierlaurent AM. Correlates of adjuvanticity: a review on adjuvants in licensed vaccines. Semin Immunol. 2018;39:14–21. https://doi.org/10.1016/j.smim.2018.05.001.
6. Kaur A, Baldwin J, Brar D, Salunke DB, Petrovsky N. Toll-like Receptor (TLR) agonists as a driving force behind next-generation vaccine adjuvants and cancer therapeutics. Curr Opin Chem Biol. 2022;70:102172. https://doi.org/10.1016/j.cbpa.2022.102172.
7. Yang J-X et al. Recent advances in the development of toll-like receptor agonist-based vaccine adjuvants for infectious diseases. Pharmaceutics. 2022;14:423. https://doi.org/10.3390/pharmaceutics14020423.
8. Didierlaurent AM et al. Adjuvant system AS01: helping to overcome the challenges of modern vaccines. Expert Rev Vaccines. 2017;16:55–63. https://doi.org/10.1080/14760584.2016.1213632.
9. Coccia M et al. Cellular and molecular synergy in AS01-adjuvanted vaccines results in an early IFNγ response promoting vaccine immunogenicity. NPJ Vaccines. 2017;2:25–14. https://doi.org/10.1038/s41541-017-0027-3.
10. Hemmi H et al. A toll-like receptor recognizes bacterial DNA. Nature. 2000;408:740–745. https://doi.org/10.1038/35047123.
11. Heeg K, Zimmermann S. CpG DNA as a Th1 trigger. Int Arch Allergy Immunol. 2000;121:87–97. https://doi.org/10.1159/000024303.
12. Scheiermann J, Klinman DM. Clinical evaluation of CpG oligonucleotides as adjuvants for vaccines targeting infectious diseases and cancer. Vaccine. 2014;32:6377–6389. https://doi.org/10.1016/j.vaccine.2014.06.065.
13. Chu RS, Askew D, Harding CV. CpG DNA switches on Th1 immunity and modulates antigen-presenting cell function. Curr Top Microbiol Immunol. 2000;247:199–210. https://doi.org/10.1007/978-3-642-59672-8_14.
14. Huang Z et al. Research progress on emulsion vaccine adjuvants. Heliyon. 2024;10:e24662. https://doi.org/10.1016/j.heliyon.2024.e24662.
15. Vono M et al. The adjuvant MF59 induces ATP release from muscle that potentiates response to vaccination. Proc Natl Acad Sci USA. 2013;110:21095–21100. https://doi.org/10.1073/pnas.1319784110.
16. Hernandez-Davies JE et al. Magnitude and breadth of antibody cross-reactivity induced by recombinant influenza hemagglutinin trimer vaccine is enhanced by combination adjuvants. Sci Rep. 2022;12:9198. https://doi.org/10.1038/s41598-022-12727-y.
17. Felgner J et al. Broad antibody and T cell responses to Ebola, Sudan, and Bundibugyo ebolaviruses using mono- and multivalent adjuvanted glycoprotein vaccines. Antiviral Res. 2024;225:105851. https://doi.org/10.1016/j.antiviral.2024.105851.
18. Gangisetty O, Reddy DS. The optimization of TaqMan real-time RT-PCR assay for transcriptional profiling of GABA-A receptor subunit plasticity. J Neurosci Methods. 2009;181:58–66. https://doi.org/10.1016/j.jneumeth.2009.04.016.
19. Jones K et al. Vaccine-linked chemotherapy improves benznidazole efficacy for acute chagas disease. Infect Immun. 2018;86:e00876-17. https://doi.org/10.1128/IAI.00876-17.
20. Hernandez-Davies JE et al. Administration of multivalent influenza virus recombinant hemagglutinin vaccine in combination-adjuvant elicits broad reactivity beyond the vaccine components. Front Immunol. 2021;12:692151. https://doi.org/10.3389/fimmu.2021.692151.
21. Kastenschmidt JM et al. Influenza vaccine format mediates distinct cellular and antibody responses in human immune organoids. Immunity. 2023;56:1910–1926.e7. https://doi.org/10.1016/j.immuni.2023.06.019.
22. Squair JW et al. Confronting false discoveries in single-cell differential expression. Nat Commun. 2021;12:5692. https://doi.org/10.1038/s41467-021-25960-2.
23. Li Y, Ge X, Peng F, Li W, Li JJ. Exaggerated false positives by popular differential expression methods when analyzing human population samples. Genome Biol. 2022;23:79. https://doi.org/10.1186/s13059-022-02648-4.
24. Jin S et al. Inference and analysis of cell-cell communication using cellchat. Nat Commun. 2021;12:1088. https://doi.org/10.1038/s41467-021-21246-9.
25. Lee RD et al. Single-cell analysis identifies dynamic gene expression networks that govern B cell development and transformation. Nat Commun. 2021;12:6843. https://doi.org/10.1038/s41467-021-27232-5.
26. Endl E, Gerdes J. The Ki-67 Protein: fascinating Forms and an Unknown Function. Exp Cell Res. 2000;257:231–237. https://doi.org/10.1006/excr.2000.4888.
27. Schröder B. The Multifaceted Roles of the Invariant Chain CD74—More than Just a Chaperone. Biochim Biophys Acta. 2016;1863:1269–1281. https://doi.org/10.1016/j.bbamcr.2016.03.026.
28. Wei H, Wang J-Y. Role of polymeric immunoglobulin receptor in IgA and IgM transcytosis. Int J Mol Sci. 2021;22:2284. https://doi.org/10.3390/ijms22052284.
29. Suzuki K, Vogelzang A, Fagarasan S. MZB1 Folding and Unfolding the Role of IgA. Proceedings of the National Academy of Sciences. 2019;116:13163–13165. https://doi.org/10.1073/pnas.1908012116.
30. Tantawy MA et al. The Interferon-Induced Gene Ifi27l2a Is Active in Lung Macrophages and Lymphocytes after Influenza A Infection but Deletion of Ifi27l2a in Mice Does Not Increase Susceptibility to Infection. PLoS One. 2014;9:e106392. https://doi.org/10.1371/journal.pone.0106392.
31. Kim GS et al. Single-Cell Analysis Identifies Ifi27l2a as a Novel Gene Regulator of Microglial Inflammation in the Context of Aging and Stroke. Res Sq. 2023;rs.3.rs-2557290. https://doi.org/10.21203/rs.3.rs-2557290/v1.

32. Lucas TM, Richner JM, Diamond MS. The Interferon-Stimulated Gene Ifi27l2a Restricts West Nile Virus Infection and Pathogenesis in a Cell-Type- and Region-Specific Manner. J Virol. 2015;90: 2600–2615. https://doi.org/10.1128/JVI.02463-15.
33. Brodziak F, Meharg C, Blaut M, Loh G. Differences in mucosal gene expression in the colon of two inbred mouse strains after colonization with commensal gut bacteria. PLoS One. 2013;8: e72317. https://doi.org/10.1371/journal.pone.0072317.
34. Holmes C, Stanford WL. Concise review: stem cell antigen-1: expression, function, and enigma. Stem Cells. 2007;25:1339–1347. https://doi.org/10.1634/stemcells.2006-0644.
35. Galaviz-Hernandez C et al. Plac8 and Plac9, novel placental-enriched genes identified through microarray analysis. Gene. 2003;309:81–89. https://doi.org/10.1016/S0378-1119(03)00508-0.
36. Blanchard E et al. Reduced expression of Tis7/IFRD1 protein in murine and human cystic fibrosis airway epithelial cell models homozygous for the F508del-CFTR mutation. Biochem Biophys Res Commun. 2011;411:471–476. https://doi.org/10.1016/j.bbrc.2011.06.104.
37. Chang M, Zhang Y, Hui Z, Wang D, Guo H. IFRD1 regulates the asthmatic responses of airway via NF-κB pathway. Mol Immunol. 2020;127:186–192. https://doi.org/10.1016/j.molimm.2020.09.010.
38. Leão FB et al. Toll-like Receptor (TLR)-induced Rasgef1b expression in macrophages is regulated by NF-κB through its proximal promoter. Int J Biochem Cell Biol. 2020;127:105840. https://doi.org/10.1016/j.biocel.2020.105840.
39. Zhao M et al. NF-κB subunits direct kinetically distinct transcriptional cascades in antigen receptor-activated B cells. Nat Immunol. 2023;24:1552–1564. https://doi.org/10.1038/s41590-023-01561-7.
40. Kober-Hasslacher M, Schmidt-Supprian M. The unsolved puzzle of C-rel in B cell lymphoma. Cancers (Basel). 2019;11:941. https://doi.org/10.3390/cancers11070941.
41. Kolmus K et al. Concurrent depletion of Vps37 proteins evokes ESCRT-I destabilization and profound cellular stress responses. J Cell Sci. 2021;134:jcs250951. https://doi.org/10.1242/jcs.250951.
42. Zamorano J, Kelly AE, Austrian J, Wang HY, Keegan AD. Costimulation of resting B lymphocytes alters the IL-4-activated IRS2 signaling pathway in a STAT6 independent manner: implications for cell survival and proliferation. Cell Res. 2001;11: 44–54. https://doi.org/10.1038/sj.cr.7290065.
43. Kelly-Welch AE et al. Transgenic expression of insulin receptor substrate 2 in murine B cells alters the cell density-dependence of IgE production in vitro and enhances IgE production in vivo1. J Immunol 2004;172:2803–2810. https://doi.org/10.4049/jimmunol.172.5.2803.
44. Kitai Y et al. Negative regulation of melanoma differentiation-associated gene 5 (MDA5)-dependent antiviral innate immune responses by arf-like protein 5B. J Biol Chem. 2015;290: 1269–1280. https://doi.org/10.1074/jbc.M114.611053.
45. Syed N et al. Transcriptional silencing of polo-like kinase 2 (SNK/PLK2) is a frequent event in B-cell malignancies. Blood. 2006;107:250–256. https://doi.org/10.1182/blood-2005-03-1194.
46. Alkallas R et al. Multi-omic analysis reveals significantly mutated genes and DDX3X as a sex-specific tumor suppressor in cutaneous melanoma. Nat Cancer. 2020;1:635–652. https://doi.org/10.1038/s43018-020-0077-8.
47. Amend SR et al. Whole genome sequence of multiple myeloma-prone C57BL/KaLwRij mouse strain suggests the origin of disease involves multiple cell types. PLoS One. 2015;10:e0127828. https://doi.org/10.1371/journal.pone.0127828.
48. Schmitz R et al. TNFAIP3 (A20) Is a tumor suppressor gene in hodgkin lymphoma and primary mediastinal B cell lymphoma. J Exp Med. 2009;206:981–989. https://doi.org/10.1084/jem.20090528.
49. Narla G et al. KLF6, a candidate tumor suppressor gene mutated in prostate cancer. Science. 2001;294:2563–2566. https://doi.org/10.1126/science.1066326.
50. Deutsch AJA et al. NR4A1-mediated apoptosis suppresses lymphomagenesis and is associated with a favorable cancer-specific survival in patients with aggressive B-cell lymphomas. Blood. 2014;123: 2367–2377. https://doi.org/10.1182/blood-2013-08-518878.
51. Doyon-Laliberté K et al. NR4A expression by human marginal zone B-cells. Antibodies (Basel). 2019;8:50. https://doi.org/10.3390/antib8040050.
52. Verstrepen L et al. Expression, biological activities and mechanisms of action of A20 (TNFAIP3). Biochem Pharmacol. 2010; 80:2009–2020. https://doi.org/10.1016/j.bcp.2010.06.044.
53. Krzyzak L et al. CD83 modulates B cell activation and germinal center responses. J Immunol. 2016;196:3581–3594. https://doi.org/10.4049/jimmunol.1502163.
54. Li Z et al. CD83: activation marker for antigen presenting cells and its therapeutic potential. Front Immunol. 2019;10:1312. https://doi.org/10.3389/fimmu.2019.01312.
55. Dubois F et al. Transcriptional meta-analysis of regulatory B cells. Eur J Immunol. 2020;50:1757–1769. https://doi.org/10.1002/eji.201948489.
56. Zheng Y et al. Regulatory T-cell suppressor program co-opts transcription factor IRF4 to control T(H)2 responses. Nature. 2009;458:351–356. https://doi.org/10.1038/nature07674.
57. Shan Q et al. Tcf1 and Lef1 provide constant supervision to mature CD8+ T cell identity and function by organizing genomic architecture. Nat Commun. 2021;12:5863. https://doi.org/10.1038/s41467-021-26159-1.
58. Nish SA et al. CD4+ T cell effector commitment coupled to self-renewal by asymmetric cell divisions. J Exp Med 2017;214: 39–47. https://doi.org/10.1084/jem.20161046.
59. Rivino L et al. Chemokine receptor expression identifies Pre-T Helper (Th)1, Pre-Th2, and nonpolarized cells among human CD4+ central memory T cells. J Exp Med. 2004;200:725–735. https://doi.org/10.1084/jem.20040774.
60. Kim MV, Ouyang W, Liao W, Zhang MQ, Li MO. The transcription factor foxo1 controls central-memory CD8+ T cell responses to infection. Immunity. 2013;39:286–297. https://doi.org/10.1016/j.immuni.2013.07.013.
61. Moser B, Schaerli P, Loetscher P. CXCR5+ T cells: follicular homing takes center stage in T-helper-cell responses. Trends in Immunology. 2002;23:250–254. https://doi.org/10.1016/S1471-4906(02)02218-4.
62. Fontenot JD, Gavin MA, Rudensky AY. Foxp3 programs the development and function of CD4+CD25+ regulatory T cells. Nat Immunol. 2003;4:330–336. https://doi.org/10.1038/ni904.
63. Hori S, Nomura T, Sakaguchi S. Control of regulatory T cell development by the transcription factor Foxp3. Science. 2003;299: 1057–1061. https://doi.org/10.1126/science.1079490.
64. Chinen T et al. An essential role for the IL-2 receptor in Treg cell function. Nat Immunol. 2016;17:1322–1333. https://doi.org/10.1038/ni.3540.
65. Wein AN et al. CXCR6 regulates localization of tissue-resident memory CD8 T cells to the airways. J Exp Med. 2019;216: 2748–2762. https://doi.org/10.1084/jem.20181308.
66. Tse S-W, Radtke AJ, Espinosa DA, Cockburn IA, Zavala F. The chemokine receptor CXCR6 is required for the maintenance of liver memory $CD8^+$ T cells specific for infectious pathogens. J Infect Dis. 2014;210:1508–1516. https://doi.org/10.1093/infdis/jiu281.
67. Kang SM et al. Transactivation by AP-1 is a molecular target of T cell clonal anergy. Science. 1992;257:1134–1138. https://doi.org/10.1126/science.257.5073.1134.
68. Feng B et al. PDE4D/cAMP/IL-23 axis determines the immunotherapy efficacy of lung adenocarcinoma via activating the IL-9 autocrine loop of cytotoxic T lymphocytes. Cancer Lett. 2023; 565:216224. https://doi.org/10.1016/j.canlet.2023.216224.
69. Cho MJ et al. Endothelial PTP4A1 mitigates vascular inflammation via USF1/A20 axis-mediated NF-κB inactivation. Cardiovasc Res. 2023;119:1265–1278. https://doi.org/10.1093/cvr/cvac193.

70. Ueda K, Arakawa H, Nakamura Y. Dual-Specificity Phosphatase 5 (DUSP5) as a direct transcriptional target of tumor suppressor P53. Oncogene. 2003;22:5586–5591. https://doi.org/10.1038/sj.onc.1206845.
71. Goel S et al. SARS-CoV-2 Switches "on" MAPK and NFκB signaling via the reduction of nuclear DUSP1 and DUSP5 expression. Front Pharmacol. 2021;12:631879. https://doi.org/10.3389/fphar.2021.631879.
72. Wu C et al. NLRP11 attenuates toll-like receptor signalling by targeting TRAF6 for degradation via the ubiquitin ligase RNF19A. Nat Commun. 2017;8:1977. https://doi.org/10.1038/s41467-017-02073-3.
73. Connolly KA et al. A reservoir of stem-like CD8+ T cells in the tumor-draining lymph node preserves the ongoing antitumor immune response. Science Immunology. 2021;6:eabg7836. https://doi.org/10.1126/sciimmunol.abg7836.
74. Okita Y et al. The transcription factor MAFK induces EMT and malignant progression of triple-negative breast cancer cells through its target GPNMB. Sci Signal. 2017;10:eaak9397. https://doi.org/10.1126/scisignal.aak9397.
75. Lee HJ et al. Genotoxic stress/P53-Induced DNAJB9 inhibits the pro-apoptotic function of P53. Cell Death Differ. 2015;22:86–95. https://doi.org/10.1038/cdd.2014.116.
76. Ramírez-Moya J et al. Identification of an interactome network between lncRNAs and miRNAs in thyroid cancer reveals SPTY2D1-AS1 as a new tumor suppressor. Sci Rep. 2022;12:7706. https://doi.org/10.1038/s41598-022-11725-4.
77. Linder A, Hagberg Thulin M, Damber J-E, Welén K. Analysis of Regulator of G-Protein Signalling 2 (RGS2) expression and function during prostate cancer progression. Sci Rep. 2018;8:17259. https://doi.org/10.1038/s41598-018-35332-4.
78. Suk F-M et al. ZFP36L1 and ZFP36L2 inhibit cell proliferation in a cyclin D-dependent and P53-independent manner. Sci Rep. 2018;8:2742. https://doi.org/10.1038/s41598-018-21160-z.
79. Png CW et al. DUSP10 regulates intestinal epithelial cell growth and colorectal tumorigenesis. Oncogene. 2016;35:206–217. https://doi.org/10.1038/onc.2015.74.
80. Jiménez-Martínez M, Stamatakis K, Fresno M. The Dual-Specificity Phosphatase 10 (DUSP10): its role in cancer, inflammation, and immunity. Int J Mol Sci. 2019;20:1626. https://doi.org/10.3390/ijms20071626.
81. Lee E et al. The pleiotropic effects of TNFα in breast cancer subtypes is regulated by TNFAIP3/A20. Oncogene. 2019;38:469–482. https://doi.org/10.1038/s41388-018-0472-0.
82. Ma F et al. SKIL facilitates tumorigenesis and immune escape of NSCLC via upregulating TAZ/autophagy axis. Cell Death Dis. 2020;11:1028–1015. https://doi.org/10.1038/s41419-020-03200-7.
83. Das T, Chen Z, Hendriks RW, Kool M. A20/tumor necrosis factor α-induced protein 3 in immune cells controls development of autoinflammation and autoimmunity: lessons from mouse models. Front Immunol. 2018;9:104. https://doi.org/10.3389/fimmu.2018.00104.
84. Agenès F, Bosco N, Mascarell L, Fritah S, Ceredig R. Differential expression of regulator of G-protein signalling transcripts and in vivo migration of CD4+ naïve and regulatory T cells. Immunology. 2005;115:179–188. https://doi.org/10.1111/j.1365-2567.2005.02146.x.
85. Augustin RC, Bao R, Luke JJ. Targeting Cbl-b in Cancer Immunotherapy. J Immunother Cancer. 2023;11:e006007. https://doi.org/10.1136/jitc-2022-006007.
86. Simonetti G et al. IRF4 controls the positioning of mature B cells in the lymphoid microenvironments by regulating NOTCH2 expression and activity. J Exp Med. 2013;210:2887–2902. https://doi.org/10.1084/jem.20131026.
87. von Werdt D et al. Regulator of G-protein signaling 1 critically supports CD8+ TRM Cell-mediated intestinal immunity. Front Immunol 2023;14:1085895., https://doi.org/10.3389/fimmu.2023.1085895.
88. Dong C et al. ICOS Co-stimulatory receptor is essential for T-Cell activation and function. Nature. 2001;409:97–101. https://doi.org/10.1038/35051100.
89. Tan Y et al. The homeoprotein Dlx5 drives murine T-cell lymphomagenesis by directly transactivating notch and upregulating Akt signaling. Oncotarget. 2017;8:14941–14956. https://doi.org/10.18632/oncotarget.14784.
90. Chen J et al. Single-cell transcriptomics reveal the intratumoral landscape of infiltrated T-Cell subpopulations in oral squamous cell carcinoma. Mol Oncol. 2021;15:866–886. https://doi.org/10.1002/1878-0261.12910.
91. Marçais A et al. Cell-autonomous CCL5 transcription by memory CD8 T cells is regulated by IL-41. J Immunol 2006;177:4451–4457. https://doi.org/10.4049/jimmunol.177.7.4451.
92. Zhu L et al. Dapl1 controls NFATc2 activation to regulate CD8+ T cell exhaustion and responses in chronic infection and cancer. Nat Cell Biol. 2022;24:1165–1176. https://doi.org/10.1038/s41556-022-00942-8.
93. McMahon CW, Raulet DH. Expression and function of NK cell receptors in CD8+ T cells. Curr Opin Immunol. 2001;13:465–470. https://doi.org/10.1016/s0952-7915(00)00242-9.
94. Peters AE, Knöpper K, Grafen A, Kastenmüller W. A multifunctional mouse model to study the role of Samd3. Eur J Immunol. 2022;52:328–337. https://doi.org/10.1002/eji.202149469.
95. Sebzda E, Zou Z, Lee JS, Wang T, Kahn ML. Transcription factor KLF2 regulates the migration of naive T cells by restricting chemokine receptor expression patterns. Nat Immunol. 2008;9:292–300. https://doi.org/10.1038/ni1565.
96. Wittner J, Schuh W. Krüppel-like Factor 2 (KLF2) in Immune Cell Migration. Vaccines (Basel). 2021;9:1171. https://doi.org/10.3390/vaccines9101171.
97. Crawford A, Angelosanto JM, Nadwodny KL, Blackburn SD, Wherry EJ. A Role for the Chemokine RANTES in Regulating CD8 T Cell Responses during Chronic Viral Infection. PLoS Pathog. 2011;7:e1002098. https://doi.org/10.1371/journal.ppat.1002098.
98. Banerji R, Saroj SD. Early Growth Response 1 (EGR1) Activation in Initial Stages of Host-Pathogen Interactions. Mol Biol Rep. 2021;48:2935–2943. https://doi.org/10.1007/s11033-021-06305-0.
99. Slade CD, Reagin KL, Lakshmanan HG, Klonowski KD, Watford WT. Placenta-specific 8 limits IFNγ production by CD4 T cells in vitro and promotes establishment of influenza-specific CD8 T cells in vivo. PLoS One. 2020;15:e0235706. https://doi.org/10.1371/journal.pone.0235706.
100. Yu S et al. Comprehensive analysis of the SLC16A gene family in pancreatic cancer via integrated bioinformatics. Sci Rep. 2020;10:7315. https://doi.org/10.1038/s41598-020-64356-y.
101. Tang Y, Xu G, Hu B, Zhu Y. HIVEP3 as a potential prognostic factor promotes the development of acute myeloid leukemia. Growth Factors. 2023;41:43–56. https://doi.org/10.1080/08977194.2022.2158329.
102. Wu Q et al. HIVEP3 inhibits fate decision of CD8+ invariant NKT cells after positive selection. J Leukocyte Biol. 2023;114:335–346. https://doi.org/10.1093/jleuko/qiad082.
103. Liu T, Zhang L, Joo D, Sun S-C. NF-κB signaling in inflammation. Signal Transduct Target Ther 2017;2:17023–17029. https://doi.org/10.1038/sigtrans.2017.23.
104. Acres RB, Conlon PJ, Mochizuki DY, Gallis B. Rapid phosphorylation and modulation of the T4 antigen on cloned helper T cells induced by phorbol myristate acetate or antigen. J Biol Chem. 1986;261:16210–16214.
105. Weyand CM, Goronzy J, Fathman CG. Modulation of CD4 by antigenic activation. J Immunol. 1987;138:1351–1354.
106. Rivas A, Takada S, Koide J, Sonderstrup-McDevitt G, Engleman EG. CD4 molecules are associated with the antigen receptor complex on activated but not resting T cells. J Immunol. 1988;140:2912–2918.
107. Petrovsky N. Comparative safety of vaccine adjuvants: a summary of current evidence and future needs. Drug Saf. 2015;38:1059–1074. https://doi.org/10.1007/s40264-015-0350-4.
108. Crotty S et al. Cutting Edge: long-term B cell memory in humans after smallpox vaccination. J Immunol. 2003;171:4969–4973. https://doi.org/10.4049/jimmunol.171.10.4969.

109. Wieten RW et al. A single 17D yellow fever vaccination provides lifelong immunity; characterization of yellow-fever-specific neutralizing antibody and T-cell responses after vaccination. PLoS One. 2016;11:e0149871. https://doi.org/10.1371/journal.pone.0149871.
110. Collins ND, Barrett ADT. Live attenuated yellow fever 17D vaccine: a legacy vaccine still controlling outbreaks in modern day. Curr Infect Dis Rep. 2017;19:14. https://doi.org/10.1007/s11908-017-0566-9.
111. Gaucher D et al. Yellow fever vaccine induces integrated multilineage and polyfunctional immune responses. J Exp Med. 2008;205:3119–3131. https://doi.org/10.1084/jem.20082292.
112. Querec TD et al. Systems biology approach predicts immunogenicity of the yellow fever vaccine in humans. Nat Immunol. 2009;10:116–125. https://doi.org/10.1038/ni.1688.
113. Hagan T et al.; Human Immunology Project Consortium (HIPC). Transcriptional atlas of the human immune response to 13 vaccines reveals a common predictor of vaccine-induced antibody responses. Nat Immunol. 2022;23:1788–1798., https://doi.org/10.1038/s41590-022-01328-6.
114. Hale JS, Ahmed R. Memory T follicular helper CD4 T cells. Front Immunol 2015;6:16., https://doi.org/10.3389/fimmu.2015.00016.
115. Luzuriaga MA, Shahrivarkevishahi A, Herbert FC, Wijesundara YH, Gassensmith JJ. Biomaterials and nanomaterials for sustained release vaccine delivery. Wiley Interdiscip Rev Nanomed Nanobiotechnol. 2021;13:e1735. https://doi.org/10.1002/wnan.1735.
116. Bobbala S, Hook S. Vaccine implants: current status and recent advancements. Emerg Top Life Sci. 2020;4:319–330. https://doi.org/10.1042/ETLS20200164.
117. Michaelides K et al. Single Administration Vaccines: Delivery Challenges, in Vivo Performance, and Translational Considerations. Expert Rev Vaccines. 2023;22:579–595. https://doi.org/10.1080/14760584.2023.2229431.
118. Quang C, Chung AW, Frazer IH, Toh ZQ, Licciardi PV. Single-Dose HPV Vaccine Immunity: Is There a Role for Non-Neutralizing Antibodies? Trends in Immunology. 2022;43:815–825. https://doi.org/10.1016/j.it.2022.07.011.
119. Jangra S et al. Sterilizing immunity against SARS-CoV-2 infection in mice by a single-shot and lipid amphiphile imidazoquinoline TLR7/8 agonist-adjuvanted recombinant spike protein vaccine. Angew Chem Int Ed Engl 2021;60:9467–9473. https://doi.org/10.1002/anie.202015362.
120. Papi A et al.; AReSVi-006 Study Group Respiratory syncytial virus prefusion f protein vaccine in older adults. N Engl J Med. 2023;388:595–608. https://doi.org/10.1056/NEJMoa2209604.
121. Chen L. Co-inhibitory molecules of the B7–CD28 family in the control of T-cell immunity. Nat Rev Immunol. 2004;4:336–347. https://doi.org/10.1038/nri1349.
122. Dyck L, Mills KHG. Immune checkpoints and their inhibition in cancer and infectious diseases. Eur J Immunol. 2017;47:765–779. https://doi.org/10.1002/eji.201646875.
123. Kim B et al. A novel therapeutic modality using CRISPR-engineered dendritic cells to treat allergies. Biomaterials. 2021;273:120798. https://doi.org/10.1016/j.biomaterials.2021.120798.
124. Zhu YX et al. The SH3–SAM Adaptor HACS1 is up-regulated in B cell activation signaling cascades. J Exp Med. 2004;200:737–747. https://doi.org/10.1084/jem.20031816.
125. Noll JE et al. SAMSN1 is a tumor suppressor gene in multiple myeloma. Neoplasia. 2014;16:572–585. https://doi.org/10.1016/j.neo.2014.07.002.
126. Tan C et al. NR4A nuclear receptors restrain B cell responses to antigen when second signals are absent or limiting. Nat Immunol. 2020;21:1267–1279. https://doi.org/10.1038/s41590-020-0765-7.
127. Chu Y et al. B cells lacking the tumor suppressor TNFAIP3/A20 display impaired differentiation and hyperactivation and cause inflammation and autoimmunity in aged mice. Blood. 2011;117:2227–2236. https://doi.org/10.1182/blood-2010-09-306019.
128. Hövelmeyer N et al. A20 deficiency in B cells enhances B-cell proliferation and results in the development of autoantibodies. Eur J Immunol. 2011;41:595–601. https://doi.org/10.1002/eji.201041313.
129. Miragaia RJ et al. Single-cell transcriptomics of regulatory T cells reveals trajectories of tissue adaptation. Immunity. 2019;50:493–504.e7. https://doi.org/10.1016/j.immuni.2019.01.001.
130. Kutty RG et al. Dual specificity phosphatase 5 is essential for T cell survival. PLoS One. 2016;11:e0167246. https://doi.org/10.1371/journal.pone.0167246.
131. Heximer SP, Cristillo AD, Forsdyke DR. Comparison of mRNA expression of two regulators of G-protein signaling, RGS1/BL34/1R20 and RGS2/G0S8, in cultured human blood mononuclear cells. DNA Cell Biol. 1997;16:589–598. https://doi.org/10.1089/dna.1997.16.589.
132. Cook ME et al. The ZFP36 family of RNA binding proteins regulates homeostatic and autoreactive T cell responses. Sci Immunol. 2022;7:eabo0981. https://doi.org/10.1126/sciimmunol.abo0981.
133. Zhang Y et al. Regulation of innate and adaptive immune responses by MAP kinase phosphatase 5. Nature. 2004;430:793–797. https://doi.org/10.1038/nature02764.
134. Tewari M et al. Lymphoid expression and regulation of A20, an inhibitor of programmed cell death. J Immunol. 1995;154:1699–1706.
135. Coornaert B et al. T Cell antigen receptor stimulation induces MALT1 paracaspase–mediated cleavage of the NF-κB inhibitor A20. Nat Immunol. 2008;9:263–271. https://doi.org/10.1038/ni1561.
136. Giannini AL, Gao Y, Bijlmakers M-J. T cell regulator RNF125/TRAC-1 belongs to a novel family of ubiquitin ligases with zinc fingers and an ubiquitin-binding domain. Biochem J. 2008;410:101–111. https://doi.org/10.1042/BJ20070995.
137. Chu P et al. Systematic identification of regulatory proteins critical for T-cell activation. J Biol. 2003;2:21. https://doi.org/10.1186/1475-4924-2-21.
138. Bai Y, Hu M, Chen Z, Wei J, Du H. Single-cell transcriptome analysis reveals RGS1 as a new marker and promoting factor for T-cell exhaustion in multiple cancers. Front Immunol. 2021;12:767070. https://doi.org/10.3389/fimmu.2021.767070.
139. Gurusamy M et al. G-protein-coupled receptor P2Y10 facilitates chemokine-induced CD4 T cell migration through autocrine/paracrine mediators. Nat Commun. 2021;12:6798. https://doi.org/10.1038/s41467-021-26882-9.
140. Paolino M, Penninger JM. Cbl-b in T-cell activation. Semin Immunopathol. 2010;32:137–148. https://doi.org/10.1007/s00281-010-0197-9.
141. Wurster AL, Withers DJ, Uchida T, White MF, Grusby MJ. Stat6 and IRS-2 cooperate in interleukin 4 (IL-4)-induced proliferation and differentiation but are dispensable for IL-4-dependent rescue from apoptosis. Mol Cell Biol. 2002;22:117–126. https://doi.org/10.1128/MCB.22.1.117-126.2002.
142. Muñoz-Fontela C, Mandinova A, Aaronson SA, Lee SW. Emerging roles of P53 and other tumour-suppressor genes in immune regulation. Nat Rev Immunol. 2016;16:741–750. https://doi.org/10.1038/nri.2016.99.
143. Zhu G et al. Mutant P53 in cancer progression and targeted therapies. Front Oncol. 2020;10:595187. https://doi.org/10.3389/fonc.2020.595187.
144. Aloni-Grinstein R, Charni-Natan M, Solomon H, Rotter V. P53 and the viral connection: back into the future. Cancers (Basel). 2018;10:178. https://doi.org/10.3390/cancers10060178.
145. Muñoz-Fontela C et al. P53 serves as a host antiviral factor that enhances innate and adaptive immune responses to influenza A virus. J Immunol. 2011;187:6428–6436. https://doi.org/10.4049/jimmunol.1101459.
146. Rivas C, Aaronson SA, Munoz-Fontela C. Dual role of P53 in innate antiviral immunity. Viruses. 2010;2:298–313. https://doi.org/10.3390/v2010298.
147. Wang J et al. RNA-seq analysis of the BCG vaccine in a humanized mouse model. Zoonoses. 2023;3:999. https://doi.org/10.15212/ZOONOSES-2022-0035.

ImmunoHorizons, 2025, 9, 1–17
https://doi.org/10.1093/immhor/vlae007
Research Article